© 2020. Published by The Company of Biologists Ltd | Journal of Cell Science (2020) 133, jcs241992. doi:10.1242/jcs.241992

RESEARCH ARTICLE

Actin waves transport RanGTP to the neurite tip to regulate non-centrosomal microtubules in neurons

Yung-An Huang[1,*], Chih-Hsuan Hsu[2,*], Ho-Chieh Chiu[2], Pei-Yu Hsi[2], Chris T. Ho[2], Wei-Lun Lo[1] and Eric Hwang[1,2,3,4,‡]

ABSTRACT

Microtubules (MTs) are the most abundant cytoskeleton in neurons, and control multiple facets of their development. While the MT-organizing center (MTOC) in mitotic cells is typically located at the centrosome, the MTOC in neurons switches to non-centrosomal sites. A handful of cellular components have been shown to promote non-centrosomal MT (ncMT) formation in neurons, yet the regulation mechanism remains unknown. Here, we demonstrate that the small GTPase Ran is a key regulator of ncMTs in neurons. Using an optogenetic tool that enables light-induced local production of RanGTP, we demonstrate that RanGTP promotes ncMT plus-end growth along the neurite. Additionally, we discovered that actin waves drive the anterograde transport of RanGTP. Pharmacological disruption of actin waves abolishes the enrichment of RanGTP and reduces growing ncMT plus-ends at the neurite tip. These observations identify a novel regulation mechanism for ncMTs and pinpoint an indirect connection between the actin and MT cytoskeletons in neurons.

KEY WORDS: Microtubules, Growth cone-like waves, Photoactivation, Neuronal development, +TIPs

INTRODUCTION

The nervous system is the main information relaying and processing unit for multicellular organisms to interact with the external world. In order for the nervous system to operate, individual neurons must be connected in a highly ordered manner. To achieve such organized connections, the developmental processes following the generation of a terminally differentiated neuron must be highly regulated. It has been shown that most, if not all, developmental processes of neurons depend on the organization and function of an essential cellular fibrous network called the microtubule (MT) cytoskeleton. MTs are tube-like polymers composed of heterodimers of α- and β-tubulins (denoted α/β-tubulin), they are also highly dynamic polymers that utilize GTP hydrolysis to control polymerization and depolymerization as well as the transition between the two phases (Brouhard and Rice, 2018; Desai and Mitchison, 1997). The ordered assembly of α/β-tubulin heterodimers gives MTs two distinct ends: a plus-end where rapid polymerization and depolymerization occur, and a minus-end where nucleation event happens. In cells actively undergoing proliferation, MT nucleation usually takes place at the centrosomes. Differentiated cells, on the other hand, largely contain non-centrosomal MTs (ncMTs) that are not organized around the centrosome (Bartolini and Gundersen, 2006; Keating and Borisy, 1999; Muroyama and Lechler, 2017; Sanchez and Feldman, 2017). In neurons, MTs are initially assembled from the centrosome (Yu et al., 1993). However, as neurons mature, the centrosome loses its MT-organizing center (MTOC) capability (Leask et al., 1997; Stiess et al., 2010). Several cellular components have been identified as the non-centrosomal MT-organizing center (ncMTOC) in neurons. Golgi outposts were first demonstrated as being able to nucleate ncMTs in dendrites of *Drosophila* da neurons (Ori-McKenney et al., 2012). However, it is important to point out that Golgi outposts are not present in all dendrites and genetically forcing Golgi outposts out of dendrites does not affect the MT organization (Nguyen et al., 2014). The augmin complex was later shown to nucleate ncMTs from the existing MTs in both the axonal and dendritic compartments (Cunha-Ferreira et al., 2018; Sanchez-Huertas et al., 2016). In line with the augmin complex discovery, another protein (TPX2) required for branch MT formation on existing MTs (Petry et al., 2013) has also been shown to promote ncMT nucleation in both axons and dendrites of mammalian neurons (Chen et al., 2017). Interestingly, the small GTPase Ran, which plays an important role in regulating TPX2 activity during mitosis has been reported to regulate TPX2-mediated ncMT nucleation in neurons (Chen et al., 2017).

Ran is a member of the Ras superfamily GTPase that is crucial in the process of nucleocytoplasmic transport (Gorlich and Mattaj, 1996). In addition to its role in nucleocytoplasmic transport, Ran has also been shown to affect spindle formation in *Xenopus laevis* egg extract (Kahana and Cleveland, 1999). The effect of Ran on mitotic spindle formation is mediated by importin-α–importin-β heterodimers, which bind to nuclear localization sequence (NLS) on spindle assembly factors (SAFs) and inhibits their activity (Clarke and Zhang, 2008). In the presence of RanGTP, SAFs are released from the inhibitory importin heterodimer and allowed to promote MT nucleation to facilitate the assembly of the mitotic spindle. One of these SAFs is the aforementioned TPX2 (Gruss et al., 2001), which can promote branching MT nucleation from existing MTs (Petry et al., 2013). Although the effect of Ran on MT nucleation is well established, most studies were carried out using meiotic egg extract or mitotic cells. The effect of Ran on MTs within post-mitotic neurons has received much less attention. A few lines of evidence indicate that Ran plays a role in neuronal morphogenesis. Firstly, Ran depletion in primary *Drosophila* neurons results in excessive neurite branching and blebbing (Sepp et al., 2008).

[1]Department of Biological Science and Technology, National Chiao Tung University, Hsinchu, Taiwan 30068. [2]Institute of Molecular Medicine and Bioengineering, National Chiao Tung University, Hsinchu, Taiwan 30068. [3]Institute of Bioinformatics and Systems Biology, National Chiao Tung University, Hsinchu, Taiwan 30068. [4]Center for Intelligent Drug Systems and Smart Bio-devices (IDS2B), National Chiao Tung University, Hsinchu, Taiwan 30068.
*These authors contributed equally to this work

‡Author for correspondence (hwangeric@mail.nctu.edu.tw)

Y.-A.H., 0000-0001-6438-2296; C.-H.H., 0000-0002-5599-807X; C.T.H., 0000-0002-7009-7704; E.H., 0000-0002-5188-581X

Handling Editor: Michael Way
Received 20 November 2019; Accepted 17 March 2020

Journal of Cell Science (2020) 133, jcs241992. doi:10.1242/jcs.241992

Secondly, Ran, RanBP1 or RCC1 (a Ran guanine nucleotide exchange factor) knockdown compromises axon specification in mammalian neurons (Mencarelli et al., 2018). Thirdly, RanGTP hydrolysis in the axoplasm has been observed after nerve injury, and perturbing the hydrolysis of RanGTP compromises the regeneration of axons (Yudin et al., 2008). These findings suggest that Ran is an important regulator of neuronal morphogenesis under both normal and injured conditions.

Neuronal actin waves (or growth cone-like waves) are actin-dependent anterograde movements along the neurite shaft that were originally discovered in cultured hippocampal neurons (Ruthel and Banker, 1998). Actin waves were later observed in organotypic hippocampal or cortical slices (Flynn et al., 2009; Katsuno et al., 2015), demonstrating that they are present both *in vitro* and *in vivo*. The neurite undergoes transient retraction when an actin wave approaches its tip; this is followed by a short period of rapid outgrowth as the actin wave reaches the tip (Ruthel and Banker, 1999). It has recently been demonstrated that the anterograde movement of the actin wave is powered by the directional polymerization (oriented toward the tip) and depolymerization (oriented toward the cell body) of membrane-associated actin filaments (Katsuno et al., 2015). This kind of propagation mechanism allows proteins associated with the actin filaments to be transported within actin waves towards the neurite tip, as a variety of actin-binding proteins, small GTPases and phosphatidylinositol-(3,4,5)-trisphosphate (PIP_3) have been documented to co-migrate with or enrich in actin waves (Kakumoto and Nakata, 2013). Although several Ras superfamily GTPases (Cdc42, Rac1 and Rap1) have been demonstrated to concentrate in actin waves (Flynn et al., 2009), whether Ran GTPase can be transported by actin waves remains unknown.

A recent discovery has shown that RanGTP is specially enriched at the tip of the neurite and around the soma (Chen et al., 2017). Furthermore, when a pharmacological perturbation disrupts the interaction between Ran and its downstream effectors, ncMT nucleation at the neurite tip is compromised. These observations raise the following questions. Firstly, is Ran GTPase able to regulate ncMT formation at any point along the neurite? Secondly, what is the mechanism by which RanGTP enrichment occurs at the neurite tip? To answer these questions, we constructed an optogenetic reagent called RanTRAP that enables the local increase of RanGTP at the photoactivation site. By photoactivating RanTRAP at a specific location along the neurite, we show that RanGTP can indeed promote ncMT formation. In addition, we detected a colocalization of RanGTP and actin waves in neurons. By examining the motility of a RanGTP-mimic mutant, we discovered that RanGTP is transported anterogradely by actin waves towards the neurite tip. Pharmacological disruption of actin waves reduces the level of RanGTP as well as decreasing the frequency at which MTs emanate at the neurite tip. These observations confirm the role of Ran GTPase in regulating ncMTs and identify a novel mechanism of moving the active RanGTP molecules towards the neurite tip.

RESULTS

Ran GTPase affects MT formation at the neurite tip

It has been reported that RanGTP is enriched in the soma and at the neurite tip (Chen et al., 2017). To confirm this localization, an antibody that specifically targets the C-terminal tail of the Ran GTPase, which is only exposed in the GTP-bound state (Richards et al., 1995), was used for immunofluorescence staining to examine dissociated hippocampal neurons at 2 days *in vitro* (2DIV) (Fig. 1A). A plasmid expressing cytosolic EGFP was transfected into neurons to serve as the cytoplasmic volume marker. The cytosolic EGFP signal was used to normalize the RanGTP signal against the cytoplasmic volume. Similar to our previous findings (Chen et al., 2017), RanGTP was found to be enriched at the tips of both axon and dendrite and in the soma (Fig. 1B). In addition, the tip of the axon exhibited a significantly higher level of RanGTP per unit volume than that of the dendrite (Fig. 1C). Interestingly, RanGTP appeared to colocalize with actin-based structures in the growth cone (Fig. 1D).

Cytoplasmic RanGTP has also been shown to activate TPX2 and to promote ncMT nucleation in neurons (Chen et al., 2017). To examine whether RanGTP regulates ncMTs, Ran mutants were utilized to alter the level of cytoplasmic RanGTP in neurons. The constitutively active Ran mutant (RanQ69L), which mimics RanGTP, was used to increase cytoplasmic RanGTP, while the dominant-negative Ran mutant (RanT24N), which irreversibly binds to the Ran guanine nucleotide exchange factors (RanGEFs) was used to reduce cytoplasmic RanGTP (Klebe et al., 1995). We first examined whether expressing RanQ69L or RanT24N altered the level of cytoplasmic RanGTP in neurons. Interestingly, expressing RanQ69L or RanT24N specifically increases or decreases RanGTP level at the neurite tip (Fig. S1A,B) without affecting its level along the neurite shaft (data not shown). We next examined the formation of growing MT plus-ends at the neurite tip in neurons expressing these Ran mutants. The CNS-enriched MT plus-end tracking protein EB3 (also known as MAPRE3) was used to assess the amount of growing MT plus-ends (Nakagawa et al., 2000). As expected, neurons expressing RanQ69L exhibit a significant increase of MT formation frequency at their neurite tips compared to those expressing wild-type Ran or RanT24N; neurons expressing RanT24N exhibit a significant decrease of MT formation frequency compared to wild-type Ran- or RanQ69L-expressing neurons (Fig. 2). On the other hand, the amount of time MT remains in the polymerization phase (persistence) and the MT polymerization rate are not affected. In addition, we discovered that expression of Ran mutants is able to alter neuronal morphogenesis (Fig. S1C,D). It is of interest to point out that neurons expressing *Aequorea coerulescens* (Ac)GFP-fused wild-type Ran show decreased neurite length compared to those expressing cytosolic AcGFP, suggesting that an overabundance of wild-type Ran can negatively affect neurite elongation. Neurons expressing the RanGTP-mimic mutant (RanQ69L) extend longer neurites than those expressing wild-type Ran, while neurons expressing RanGDP-mimic mutant (RanT24N) possess shorter neurites than wild-type Ran-expressing ones (Fig. S1C,D). Neurite branching is not significantly altered by the expression of Ran mutants (Fig. S1D), and this is probably due to the low branching capability at such an early stage. On the other hand, neurons expressing RanT24N sprout fewer primary neurites than those expressing RanQ69L or wild-type Ran (Fig. S1D). Taken together, these findings indicate that a change in the level of RanGTP at the neurite tip alters the amount of polymerizing ncMT plus-ends at this location and affects the overall morphology of the neuron.

A photoactivatable Ran promotes MT formation along the neurite

We have shown that expressing Ran mutants alters the level of cytoplasmic RanGTP at the neurite tip and leads to a change in the amount of growing ncMT plus-ends at this location. To demonstrate that Ran GTPase is a major regulator of ncMTs, it is important to show that RanGTP can induce ncMT formation in other regions of the neuron. Since altering the level of cytoplasmic RanGTP can lead

Journal of Cell Science (2020) 133, jcs241992. doi:10.1242/jcs.241992

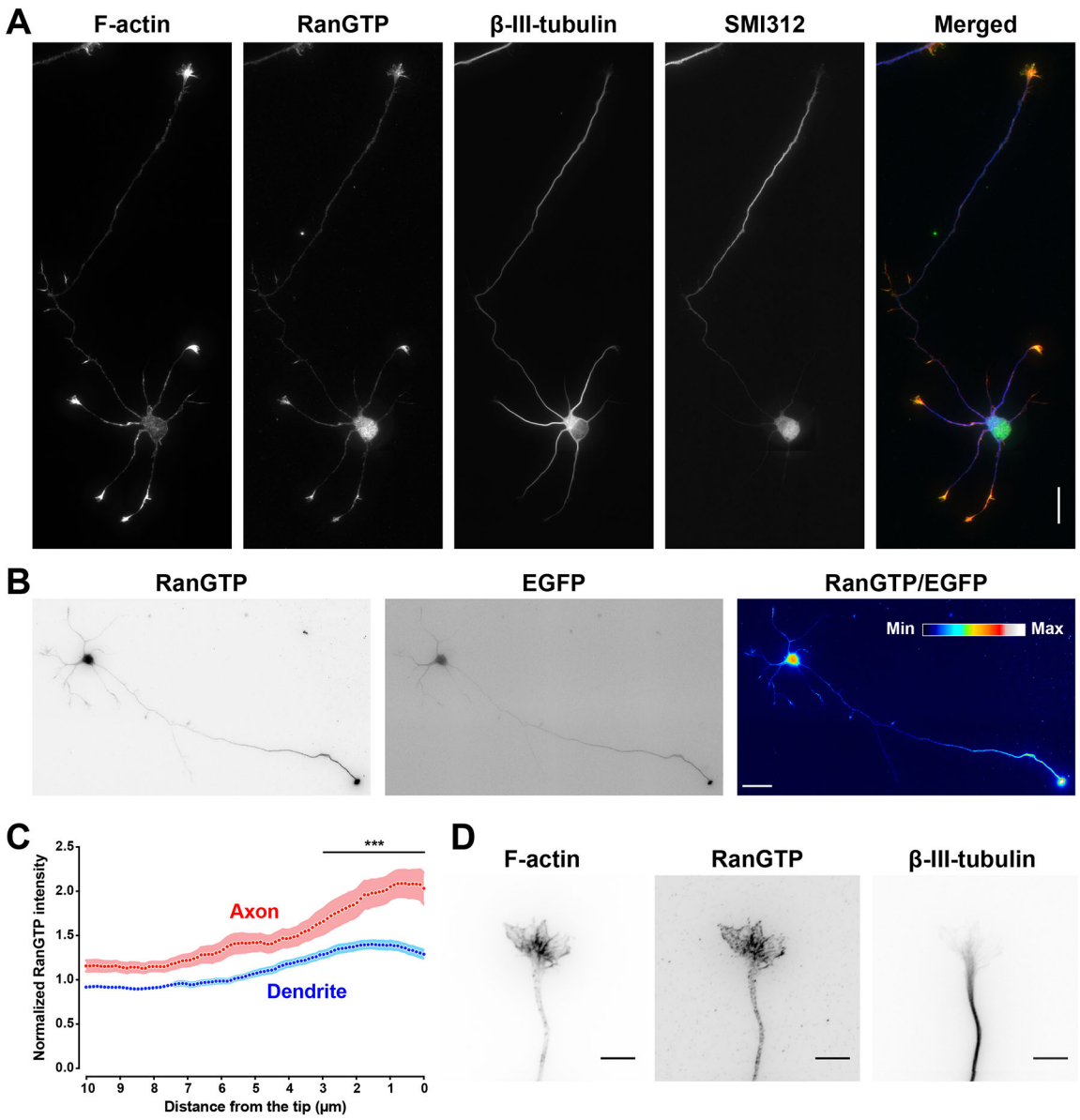

Fig. 1. GTP-bound Ran is enriched in both the axon and dendrite tips, and colocalizes with actin-based structures. (A) Representative images of a 2DIV hippocampal neuron immunofluorescence stained for RanGTP, β-III-tubulin, SMI312 antibodies and phalloidin. The merged image shows phalloidin staining in red, RanGTP in green and β-III-tubulin in blue. Stitching of the different image fields was performed automatically by the microscope software (Nikon NIS-Elements v. 4.13.05). Scale bar: 25 µm. (B) Representative images of a 2DIV hippocampal neuron with cytosolic EGFP immunofluorescence stained with anti-RanGTP antibody. The ratio image is pseudo-colored. Scale bar: 30 µm. (C) Cytoplasmic volume-normalized RanGTP intensity linescan along a 10 µm stretch from axon (red) or dendrite (blue) tips in 2DIV hippocampal neurons. Dots and shaded areas indicate mean and s.e.m. collected from 57 axons and 194 dendrites. ***P<0.001 (two-way ANOVA followed by Sidak post-hoc analysis). (D) Representative image of the growth cone from a 2DIV hippocampal neuron fixed and stained with RanGTP (middle), β-III-tubulin (right) antibody and phalloidin (left). Images were inverted to facilitate visualization. Scale bars: 10 µm.

to detrimental effects on cell survival due to its influence on nucleocytoplasmic transport, it is therefore crucial to have the capability of controlling the location of RanGTP production with spatial precision, which would then allow an examination of its effect on ncMTs. To achieve this goal, we utilized the LOVTRAP system developed in Klaus Hahn's laboratory (Wang et al., 2016). This system takes advantage of a photoreactive domain called LOV2 that is derived from phototropins in plants (Huala et al., 1997; Salomon et al., 2000). In the absence of light, the LOV2 domain binds to a short peptide derived from the Z subunit of protein A called Zdark (ZDK). Upon blue light irradiation, a conformational change in the LOV2 domain causes it to dissociate from ZDK. By fusing the LOV2 domain to an organelle-targeting sequence and fusing ZDK to the protein of interest, one can sequester this protein of interest to a specific organelle in the dark and release it at the specific time and location desired upon light irradiation. We used this system to design an optogenetic tool called 'RanTRAP' to spatially control the level of RanGTP. Our RanTRAP system is composed of two parts: a mitochondrial targeting sequence fused to the LOV2 domain (NTOM20–LOV2) and the aforementioned RanGTP-mimic RanQ69L fused to the ZDK and mCherry (mCherry–ZDK–RanQ69L). In the absence of light, mCherry–ZDK–RanQ69L binds to NTOM20–LOV2 and this sequesters the activity of this RanGTP-mimic mutant to the mitochondria. Upon light irradiation, LOV2 and ZDK dissociate from each other, releasing mCherry–ZDK–RanQ69L from the mitochondria.

Journal of Cell Science (2020) 133, jcs241992. doi:10.1242/jcs.241992

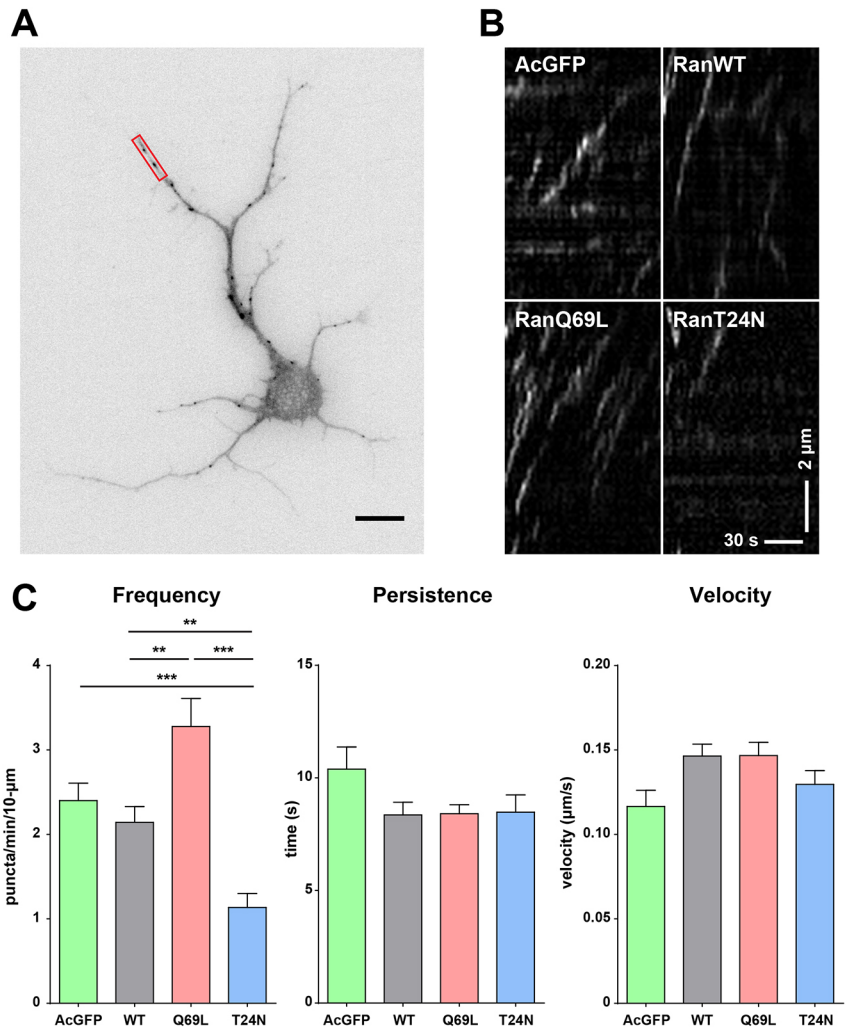

Fig. 2. Ran mutants affect the formation of growing microtubule plus-ends at the neurite tip. (A) Representative images of 2DIV dissociated cortical neurons co-expressing AcGFP–RanWT and EB3–mCherry; only the EB3–mCherry channel is shown. The red box indicates the region where kymographs were generated. Scale bar: 10 µm. (B) Representative kymographs of EB3–mCherry at the tip of the neurite in various Ran mutants expressing neurons. (C) Quantification of EB3–mCherry dynamics in AcGFP (green), AcGFP-RanWT (gray), AcGFP-RanQ69L (red), and AcGFP-RanT24N (blue)-expressing neurons. More than eight neurites from six neurons were analyzed per condition per repetition. $^{**}P<0.01$, $^{***}P<0.001$ (one-way ANOVA followed by Tukey's post-hoc test). Error bars represent s.e.m. from three independent experiments.

mCherry–ZDK–RanQ69L then binds to importin-β and disrupts the inhibitory importin complex. This leads to the activation of TPX2 and the nucleation of ncMTs (Fig. 3A). In addition to the RanGTP-mimic RanQ69L, the RanGDP-mimic RanT24N was also fused to ZDK to serve as the control. These constructs are referred to as RanQ69L-TRAP and RanT24N-TRAP hereafter.

We first validated this RanTRAP platform by examining whether it can mask the phenotypic effect of RanQ69L expression or RanT24N expression in mitotic cells. It has been shown that overexpressing the constitutively active RanQ69L or the dominant-negative RanT24N leads to the formation of abnormal mitotic spindles (Moore et al., 2002). We reasoned that if this RanTRAP tool can sequester these Ran mutants to the mitochondria, these mutants should not be able to bring about the formation of abnormal spindles. To increase the mitotic index of HeLa cells, double thymidine arrest was utilized to synchronize these cells (Fig. S2A). Next, the mitotic spindle morphology and chromosome alignment in mitotic HeLa cells expressing either RanQ69L-TRAP or RanT24N-TRAP were examined. Abnormal mitotic spindles were classified into three main categories: (1) bipolar spindles with misaligned chromosomes, (2) multipolar spindles, or (3) monopolar spindles (Fig. S2B). In cells expressing mCherry–ZDK–RanQ69L or mCherry–ZDK–RanT24N alone, the percentage of HeLa cells with abnormal spindle is significantly higher than in untransfected cells, demonstrating that mCherry–ZDK–Ran mutants cause abnormal mitotic spindle formation in our hands. In contrast, cells expressing NTOM20–LOV2-WT (NTOM20 fused to the wild-type LOV2) exhibit a low percentage of abnormal spindles, similar to what is seen in untransfected cells. In cells co-expressing NTOM20–LOV2-WT and the mCherry–ZDK–Ran mutant, the percentage of cells with abnormal spindles is significantly lower than for cells expressing the mCherry–ZDK–Ran mutant alone or those co-expressing NTOM20–LOV2-I539E (a mutant LOV2 that always stays in the photoactivated conformation) (Harper et al., 2004) and the mCherry–ZDK–Ran mutant (Fig. S2C); these results confirm that sequestering Ran protein onto the mitochondria can block its function. Taken together, these findings demonstrate that the RanTRAP system does inhibit the function of Ran mutants in the absence of light.

We next examined whether RanTRAP can target Ran mutants onto the mitochondria present within neurites. When NTOM20–mVenus–LOV2-WT was introduced into mouse cortical neurons, it was found to colocalize with MitoTracker signals in the neurite (Fig. S3A), indicating that NTOM20–mVenus–LOV2-WT is targeted onto the mitochondria. When the plasmid expressing NTOM20–mVenus–LOV2-WT and the plasmid expressing mCherry–ZDK–Ran were co-transfected into dissociated neurons, colocalization was also detected along the neurite (Fig. S3B). These results demonstrate that the mitochondrion is an ideal organelle to target and sequester Ran mutants within neurites. Furthermore, it has been documented that the molar ratio of LOV2- to ZDK-fused proteins is crucial for achieving maximal release of the trapped protein upon irradiation (Wang and

Journal of Cell Science (2020) 133, jcs241992. doi:10.1242/jcs.241992

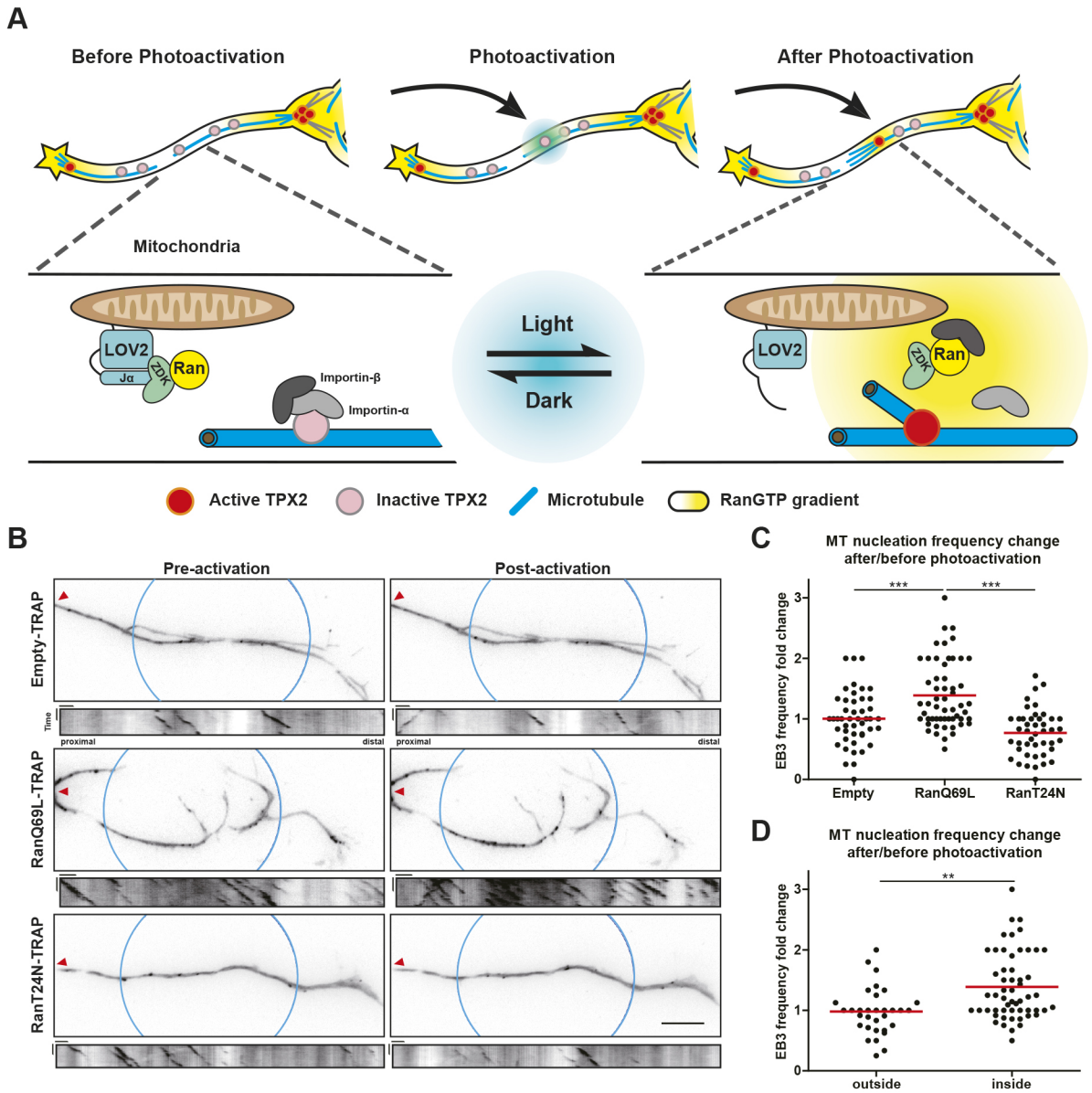

Fig. 3. Local production of RanGTP promotes the formation of growing microtubule plus-ends along the neurite. (A) Schematic illustration of local photoactivation of RanTRAP and its promotion of non-centrosomal microtubule formation along the neurite. (B) Representative images and kymographs of 4DIV mouse hippocampal neurons expressing EB3–mCherry and Empty-TRAP (top), RanQ69L-TRAP (middle) or RanT24N-TRAP (bottom). Blue circles indicate the region of photoactivation that were used to generate kymographs. The red arrowheads denote the proximal side of the neurite. All images have the same scale and the scale bar represents 10 µm. In all kymographs, vertical scale bars represent 15 s and horizontal scale bars represent 2 µm. (C) Quantification of EB3–mCherry frequency fold change (after:before) in photoactivated regions. The red horizontal bars indicate the mean frequency. This result was obtained from three or four (four for the RanQ69L-TRAP group) independent experiments. ***P<0.001 (one-way ANOVA followed by Tukey's post-hoc analysis). (D) Quantification of EB3–mCherry frequency fold change (after:before) in regions inside or outside the photoactivation in neurons expressing RanQ69L-TRAP and EB3–mCherry. The red horizontal bars indicate the mean frequency. This result was obtained from four independent experiments. **P<0.01 (two-tailed Student's t-test).

Hahn, 2016). Since the molar ratio of LOV2- and ZDK-fused proteins cannot be readily determined, the molar ratio of the two expression plasmids was used to empirically test how to achieve maximal release upon irradiation (Fig. S4).

Next, we sought to determine whether locally photoactivating RanTRAP-expressing neurons can release the RanGTP-mimic mutant within the light-irradiated region of the neurite. In this experiment, plasmids expressing NTOM20–mVenus–LOV2-WT and mCherry-ZDK–RanQ69L (RanQ69L-TRAP) were transfected into dissociated neurons. The dynamic localization of mCherry-ZDK–RanQ69L before and after local photoactivation was then examined. Upon local photoactivation, mCherry-ZDK–RanQ69L was immediately released from the mitochondria into the cytosol. This cytosolic pool of mCherry-ZDK–RanQ69L then gradually reassociated back to the mitochondria (Fig. S5). This result shows that spatial and reversible release of RanGTP along the neurite can be achieved in dissociated neurons.

Finally, to confirm whether the cytoplasmic RanGTP can promote ncMT plus-end growth in neurons, the photoactivatable RanTRAP system was utilized to locally release RanGTP within the photoactivated region along the neurite. We reason that if RanGTP does promote ncMT formation, releasing the RanGTP-mimic

Journal of Cell Science (2020) 133, jcs241992. doi:10.1242/jcs.241992

RanQ69L will cause an increase of growing MT plus-ends within the photoactivated region (Fig. 3A). To examine MT plus-end growth, EB3–mCherry was used to label the growing MT plus-ends. A 24-pulse regime (24 pulses of 80 ms irradiation with 5 s duration in between pulses) was established to generate a sustained level of RanGTP for ∼2 min at the photoactivation region. This 2-min time period was selected based on the observation that adding RanQ69L and TPX2 dramatically enhances MT nucleation within 66 s in *Xenopus* egg extract (Petry et al., 2013). To maximize the effect of RanTRAP, photoactivation was carried out in regions of neurites more than 15 µm from either the soma or the neurite tip, where endogenous RanGTP level is low (Chen et al., 2017). EB3–mCherry dynamics was quantified before and after photoactivation (Fig. 3B; Movies 1–3). As expected, photoactivating neurons co-expressing NTOM20–mVenus–LOV2-WT and RanQ69L-TRAP leads to a significant increase in EB3–mCherry comets in the irradiated region compared to photoactivating neurons co-expressing NTOM20–mVenus–LOV2-WT and mCherry-ZDK (Empty-TRAP) (Fig. 3C). Furthermore, the increase in EB3–mCherry comets after photoactivation only occurs in the irradiated region (Fig. 3D). On the other hand, photoactivating neurons expressing NTOM20–mVenus–LOV2-WT and the RanGDP-mimic mCherry–ZDK–RanT24N (RanT24N-TRAP) does not significantly alter the frequency of EB3–mCherry comets (Fig. 3C). These results demonstrate that the local release of RanGTP by itself can enhance the formation of growing ncMT plus-ends along neurites, indicating that the cytoplasmic Ran is the major regulator of ncMT in neurons.

Actin waves transport GTP-bound Ran towards the neurite tip

The localization of RanGTP at the neurite tip (Fig. 1) prompted us to determine the mechanism of tip enrichment. Two possible mechanisms can be put forward to explain the tip-enriched RanGTP localization. Firstly, it is possible that an unknown RanGEF localizes to the neurite tip and locally produces RanGTP molecules. Alternatively, RanGTP molecules could be produced elsewhere (potentially in the soma) and transported into the neurite towards the neurite tip. Our results argue against the first mechanism because a RanGTP-mimic mutant is enriched at the neurite tip while a RanGDP-mimic mutant is essentially absent at the neurite tip when each is expressed in neurons independently (Fig. S1A,B). Since RanGEFs have a higher affinity towards RanGDP than RanGTP, a tip-localized RanGEF should cause the enrichment of RanGDP instead of RanGTP at the neurite tip. On the other hand, several observations support the RanGTP transportation mechanism. First, we detected the colocalization of RanGTP with an actin-based structure in the growth cone (Fig. 1C). Second, the amount of polymerizing MTs has been observed to increase immediately behind actin waves (Winans et al., 2016). Given that actin waves are responsible for the anterograde transport of a range of biological molecules (Inagaki and Katsuno, 2017), we hypothesize that they are also involved in moving RanGTP molecules towards the neurite tips. It is possible that the increased amount of polymerizing MTs observed by Winan and colleagues is caused by RanGTP moving with actin waves and causing ncMT formation in its wake. As a first step towards confirming the RanGTP transportation hypothesis, we examined the involvement of the actin cytoskeleton in the tip localization of RanGTP. Dissociated neurons (1DIV) were treated with 2.5 µM cytochalasin D for 6 h to depolymerize actin filaments; this treatment has been shown to compromise actin-based structures in neurites without affecting neurite formation or elongation (Chia et al., 2016). While actin filaments in DMSO-treated control neurons are unaffected, they are largely absent from the growth cones of cytochalasin D-treated neurons (Fig. 4A,B). In addition, RanGTP was no longer enriched at the neurite tip in cytochalasin D-treated neurons (Fig. 4C,D). This result indicates that the actin-based structures are responsible for the enrichment of RanGTP at the neurite tips.

Given that actin waves have been documented to transport various cellular cargoes in neurons (Inagaki and Katsuno, 2017) and that neurite tip enrichment of RanGTP depends on actin-based structures, actin waves are an attractive candidate for the transportation of RanGTP. To determine whether actin waves are the driving force behind the anterograde transport of RanGTP, we first examined the localization of RanGTP and actin waves in fixed neurons. In addition to its high abundance in the growth cone, RanGTP also colocalized with the actin wave (Fig. 5A,B). Consistent with a previous observation (Winans et al., 2016), βIII-tubulin signal intensity can be seen to increase in and behind the actin wave (Fig. 5B). By normalizing the RanGTP signal against the cytoplasmic volume (using cytosolic EGFP expressed from a plasmid), we can reject the possibility that the increase of RanGTP at the actin wave is due to the increase of cytoplasmic volume (Fig. S6). In addition to using fixed neurons, we examined the motility of RanQ69L (RanGTP-mimic) in young neurons that are actively generating actin waves (Flynn et al., 2009; Ruthel and Banker, 1999). Plasmids expressing AcGFP–RanQ69L, AcGFP–RanT24N, or cytosolic AcGFP were introduced into dissociated neurons just before plating, and the motility of the AcGFP signal as well as the actin waves was monitored at 2DIV through live-cell imaging. Consistent with our RanGTP transportation hypothesis, AcGFP–RanQ69L can be observed to move anterogradely in clusters along the neurite and co-migrate with the actin wave towards the tip (Fig. 5C,F; Movie 4). In contrast, AcGFP–RanT24N exhibits minimal signal in the neuronal cytoplasm and does not co-migrate with the actin wave (Fig. 5D,G; Movie 5). To eliminate the possibility that the co-migration of RanQ69L with actin waves is due to the increase in the cytoplasmic volume around the wave, we also examined the motility of cytosolic AcGFP (Fig. 5E,H; Movie 6). While the cytosolic AcGFP signal increased in the presence of the actin wave, this increase of AcGFP signal was also detected behind the actin wave. This is consistent with a previous observation showing that actin waves widen the neurite shaft (Winans et al., 2016), and argues against the possibility that the co-migration of RanQ69L with actin waves is due to the increase in the cytoplasmic volume around the wave. To quantify the degree of co-migration between Ran mutant and the actin wave, we measured the AcGFP signal in a selected region of interest (ROI) along the neurite that experienced an actin wave from 15 min before to 15 min after the arrival of the actin wave. The time at which the actin wave passes through the ROI is set to 0 min (Fig. 5I). If the AcGFP-tagged protein co-migrates with the actin wave, one would expect the signal intensity of AcGFP to peak at the time of the actin wave passage. This is indeed the case for the AcGFP–RanQ69L signal (Fig. 5J). In contrast, the AcGFP–RanT24N signal did not peak at 0 min. It should be noted that the large fluctuation in the AcGFP–RanT24N signal over time is due to its low intensity in the neuronal cytoplasm. Interestingly, while cytosolic AcGFP exhibits peak intensity when the actin wave passes through the ROI, its relative intensity at the peak is significantly lower than that of AcGFP–RanQ69L. This indicates that AcGFP–RanQ69L is significantly more enriched in the actin wave than the cytosolic AcGFP molecule. Taken together, our findings demonstrate that RanGTP is transported by actin waves towards the neurite tip.

Journal of Cell Science (2020) 133, jcs241992. doi:10.1242/jcs.241992

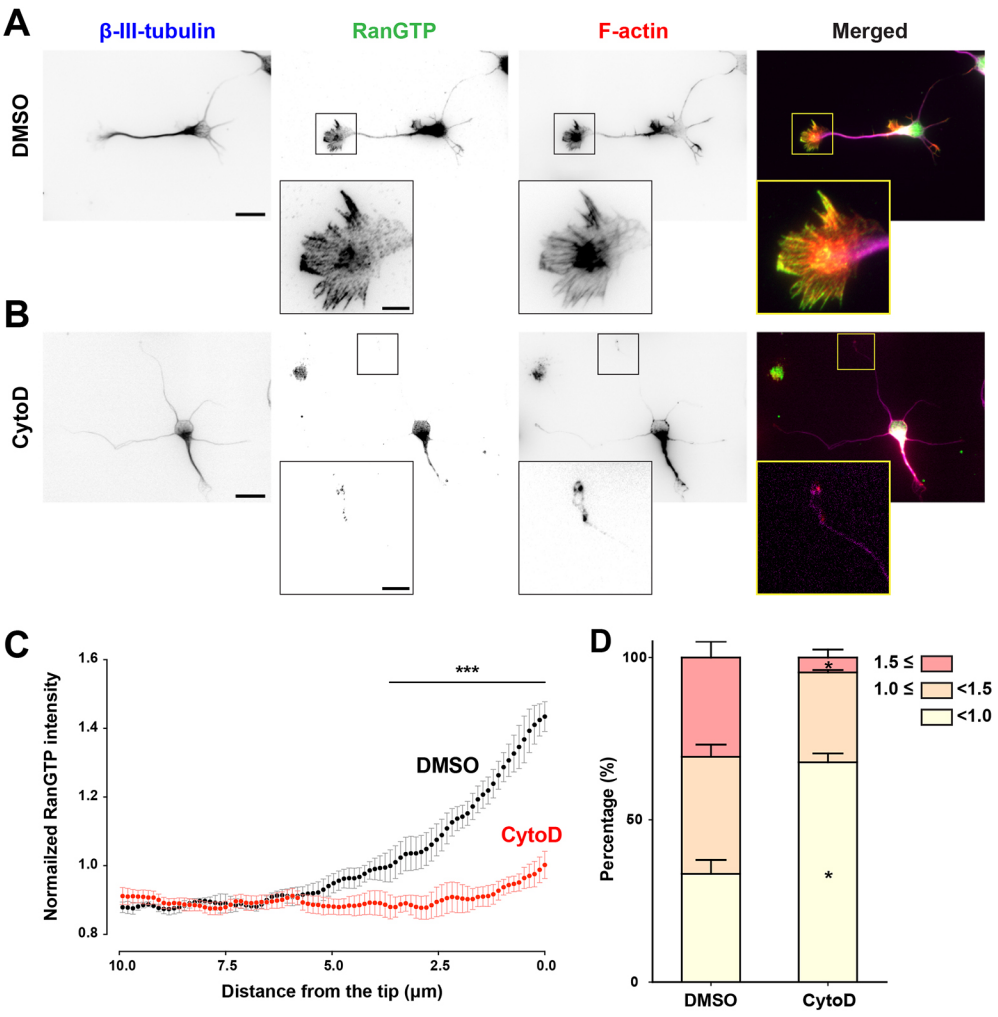

Fig. 4. The localization of RanGTP at the neurite tip depends on the actin cytoskeleton. Representative images of 1DIV hippocampal neurons treated with DMSO (A) or 2.5 µM cytochalasin D (CytoD) (B) for 6 h. The boxed areas at the neurite tips are magnified in the insets. The scale bars represent 20 µm and 5 µm in insets. (C) Normalized RanGTP level linescans along a 10 µm stretch from the neurite tip in DMSO (black)- and 2.5 µM cytochalasin D (red)-treated neurons. RanGTP intensity is normalized against the mean intensity along the entire neurite. The dots and error bars indicate mean±s.e.m. from three independent experiments. ***P<0.001 (two-way ANOVA followed by Bonferroni post-hoc analysis). (D) Quantification of the RanGTP intensity ratio at the neurite tip. The mean intensity of RanGTP within 1 µm of the neurite tip was divided by the intensity along the entire neurite. RanGTP intensity ratios are classified into three groups: the group with ratio equal to or greater than 1.5 is shown in red, the group with ratio between 1.5 and 1.0 is shown in orange, and the group with ratio below 1.0 is shown in yellow. *P<0.05 (two-tailed Student's t-test). Error bars represent s.e.m. from three independent experiments involving a total of 135 and 141 neurites from either DMSO- or cytochalasin D-treated neurons, respectively.

Disrupting actin cytoskeleton reduces microtubule formation at the neurite tip

Given that RanGTP is responsible for promoting growing ncMT plus-end formation and the fact that it is transported by actin waves towards the neurite tip, the logical outcome of disrupting the propagation of actin waves is that there should be a reduction in growing ncMT plus-ends at the tips of the neurites. We set out to test this hypothesis by treating neurons with 2.5 µM cytochalasin D for 6 h, a condition previously shown to eliminate actin waves and to significantly reduce RanGTP at the neurite tip (Fig. 4). Differential interference contrast (DIC) microscopy was used to identify the tips of the neurites. While cytochalasin D treatment does not affect the amount of polymerizing MT plus-ends within the soma (Fig. 6A,D), the treatment does cause a significant reduction in growing MT plus-ends at the neurite tip (Fig. 6B,C; Movies 7,8). Furthermore, cytochalasin D treatment only reduces the amount of growing MT plus-ends, but does not affect MT polymerization velocity or the time MTs spend in the polymerization phase (Fig. 6C). These findings show that ncMT formation at the neurite tip is influenced by the actin cytoskeleton. Given that both actin waves and actin-based structure in the growth cone are disrupted by cytochalasin D treatment, our data suggest that the actin cytoskeleton is crucial for either the transportation or anchoring (or both processes) of RanGTP in neurons and provide a new indirect connection between these two cytoskeleton structures.

DISCUSSION

Recent investigations have started to uncover the cellular components that are crucial for the nucleation of ncMTs in neurons; nevertheless, no regulatory mechanism has yet to be identified. Here, we show that the small GTPase Ran plays an important role in controlling ncMTs along the neurite. We have first shown that expressing either the RanGTP- or RanGDP-mimic mutant can specifically increase or decrease the RanGTP level at the tip of the neurite; this in turn enhances or reduces the amount of polymerizing ncMT plus-ends at the neurite tip. To demonstrate that Ran can regulate ncMT formation in regions other than the neurite tip, we constructed an optogenetic tool called RanTRAP that allows the release of the RanGTP-mimic mutant protein within the photoactivation region. By photoactivating RanTRAP along the neurite shaft where endogenous RanGTP levels are low, we demonstrated that the Ran GTPase is indeed able to control ncMT formation in neurons. In addition, we identified a novel transport mechanism for RanGTP in neuronal cytoplasm. First, it was observed that the endogenous RanGTP colocalizes with actin waves in fixed neurons. Second, disrupting actin wave propagation using cytochalasin D essentially eliminated RanGTP enrichment at the neurite tip. Finally, the co-migration of the AcGFP-tagged RanGTP-mimic mutant protein and the actin wave was observed in live neurons. These observations demonstrate that the actin wave is a major contributor to the enrichment of RanGTP at neurite tips. Consistent with the idea that RanGTP promotes the formation of growing ncMT plus-ends and that it is transported by actin waves to

Journal of Cell Science (2020) 133, jcs241992. doi:10.1242/jcs.241992

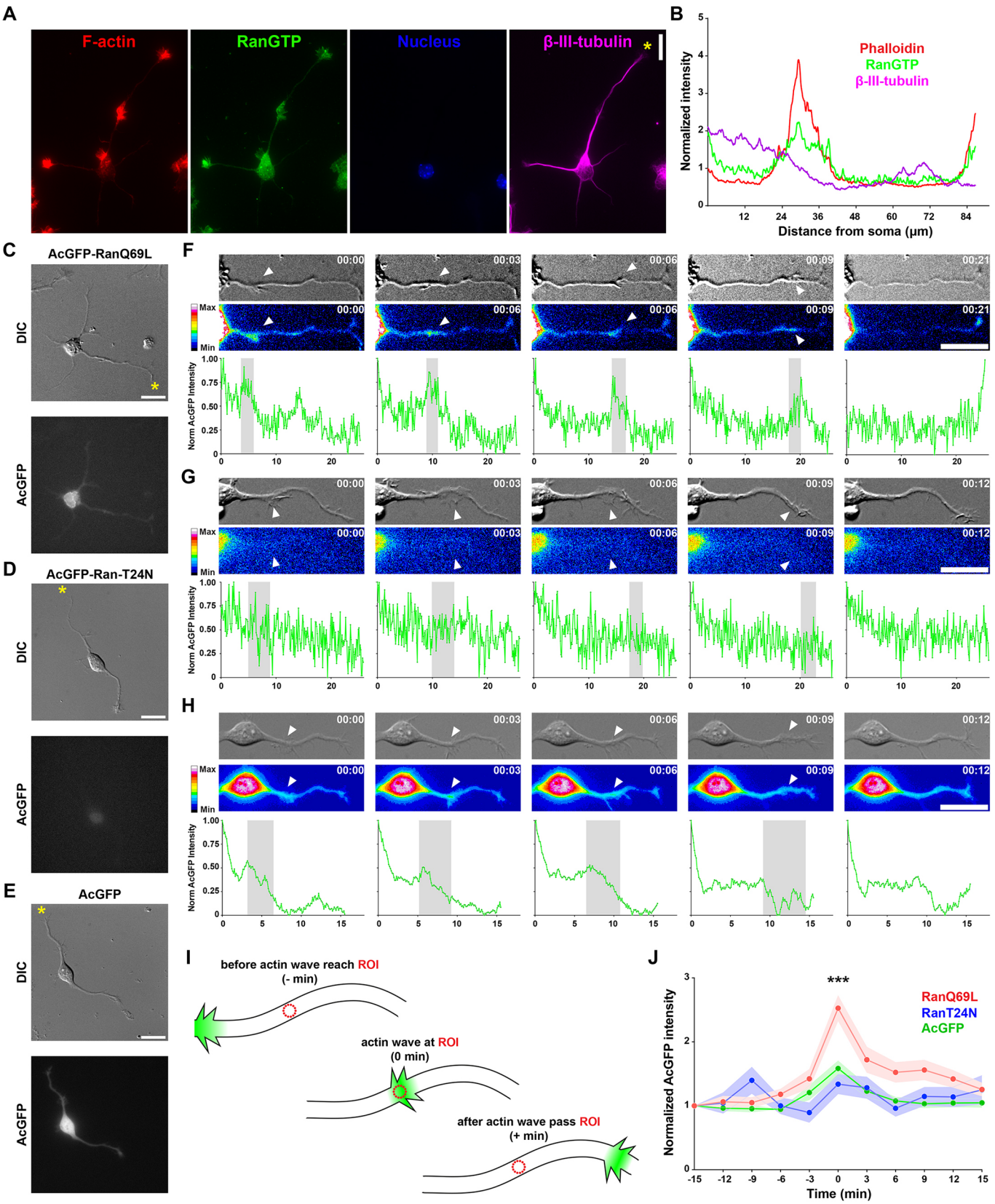

Fig. 5. See next page for legend.

the neurite tip, cytochalasin D treatment, which abolishes actin waves, also causes a significant reduction in amount of growing ncMT plus-ends at the neurite tip.

Given that γ-tubulin, augmin and TPX2 interact with each other and that MT nucleation from the sides of existing MTs requires all three proteins in *Xenopus* egg extract (Petry et al., 2013), it is

Journal of Cell Science

Journal of Cell Science (2020) 133, jcs241992. doi:10.1242/jcs.241992

Fig. 5. GTP-bound Ran is transported by actin waves towards the neurite tip. (A) Representative images of 1DIV hippocampal neurons immunofluorescence stained with antibodies against RanGTP (green) and the neuron-specific β-III-tubulin (purple). Actin filaments and the nucleus were stained with phalloidin (red) and DAPI (blue), respectively. Scale bar: 20 µm. (B) The intensity linescan of indicated molecules along the asterisked neurite in A. (C–E) Representative images of actin waves containing 2DIV cortical neurons expressing AcGFP–RanQ69L (C), AcGFP–RanT24N (D) or AcGFP (E). Scale bars: 10 µm. (F–H) Time-lapse DIC (top) and AcGFP (middle) images, as well as the AcGFP intensity linescan (bottom) of a single neurite from neurons expressing AcGFP–RanQ69L (F), AcGFP–RanT24N (G) or AcGFP (H). Neurite segments in F–H are derived from the asterisked neurite in C–E, respectively. The white arrowheads mark the location of the actin wave. The time stamps (hour:min) indicate the time progressed since the first image. The gray shaded area in the linescan graphs indicates the location of the actin wave. The *x*-axis of the linescan graphs indicates the distance (in µm) from the base of the neurite. Scale bars: 10 µm. (I) Schematic illustration of the method for quantifying the AcGFP intensity fluctuation over time in a selected ROI along the neurite shaft. The dotted circles indicate the selected ROI where the AcGFP signal (green glow) was measured. (J) Quantification of the AcGFP intensity fluctuation in the selected ROIs along the neurite shaft from 15 min before to 15 min after the arrival of the actin wave. The time at which the actin wave passes through the selected ROI is set to 0 min. ***P<0.001 (two-way ANOVA followed by Tukey post-hoc analysis between RanQ69L and RanT24N as well as between RanQ69L and AcGFP). Dots and shaded areas indicate mean and s.e.m. More than 22 actin wave-containing neurites were analyzed in each condition from three independent experiments.

tempting to speculate that RanGTP promotes ncMT nucleation by releasing TPX2 from its inhibitory importin heterodimers which in turn activates the γ-tubulin–augmin–TPX2 complex at the neurite tip. In support of this hypothesis, TPX2 and augmin complex subunits have been observed to localize along neurites (Chen et al., 2017; Cunha-Ferreira et al., 2018). In addition, both importin-α and importin-β molecules have been observed to present throughout the cytoplasm in cultured neurons (Chen et al., 2017; Hanz et al., 2003). Furthermore, Ran–importin-β complexes have been detected in the soma and the neurite tips of hippocampal neurons (Chen et al., 2017). It will be interesting to test whether the γ-tubulin–augmin–TPX2 complex is present at various places along neurites and whether Ran also regulates augmin-mediated ncMT nucleation.

The observation that the local release of RanGTP along the neurite shaft leads to growing ncMT plus-end formation at the releasing site suggests neurons may utilize Ran to dynamically reorganize their MT network. It is currently unclear if and how neurons can control the localization of Ran within different regions. One possibility is the utilization of RanGTP-anchoring protein(s) to trap RanGTP at specific regions within the neuron. For example, RanBP9 is a RanGTP-binding protein that has been shown to cause ectopic MT nucleation when overexpressed (Nakamura et al., 1998). In addition, RanBP9 has been observed to localize along the neurite (Lakshmana et al., 2012). If we consider that Ran depletion leads to morphological changes in neurons (Mencarelli et al., 2018; Sepp et al., 2008), it seems likely that locally elevating the level of RanGTP will also alter the morphology of the neuron. It will be interesting to test this hypothesis by long-term RanQ69L-TRAP photoactivation along the neurite shaft to see if this can lead to the formation of a collateral branch.

The discovery that RanGTP is transported by actin waves towards the neurite tip provides a novel mechanism for cells to position this cytosolic small GTPase. While the effect of Ran GTPase on positioning the actin cytoskeleton has previously been observed in *Xenopus* egg (Deng et al., 2007; Yi et al., 2011), the effect of the actin cytoskeleton on positioning Ran GTPase has never been described. It is interesting to point out that an increase in plus-end binding protein EB1 and MT density can be detected immediately behind the actin wave (Winans et al., 2016), and it has been hypothesized that actin waves make the neurite wider to create a larger space for more MTs to form in. Perhaps the increase in growing MT plus-ends and MT density can also be attributed to the effect of RanGTP moving along with the actin wave, causing ncMT formation in its wake. In order for RanGTP to be transported by the actin wave, specific adapter protein(s) that are localized to the actin wave and interact with RanGTP must be present. As of now, the identity of these adapter protein(s) remains unknown. One potential candidate for this adapter is the protein ezrin, an actin-binding protein that is concentrated within the actin waves (Ruthel and Banker, 1998). Ezrin has been shown to interact with the cytoplasmic domain of L1CAM (Dickson et al., 2002), a neural cell adhesion molecule that also interacts with the Ran-binding protein RanBP9 to regulate neurite outgrowth (Cheng et al., 2005; Woo et al., 2012). RanBP9 has been shown to selectively bind to RanGTP in a yeast two-hybrid screen (Nakamura et al., 1998). Collectively, the above findings suggest an ezrin–L1CAM–RanBP9 complex may act as the adapter for the transport of RanGTP within actin waves. In addition to the involvement of adapter proteins within the actin wave, we also believe that specific RanGTP-anchoring protein(s) are very likely to exist at the neurite tip in order for RanGTP to be enriched at this location. This is because the frequency of actin wave generation (1–2 waves per hour) is much too low to maintain an elevated pool of cytosolic RanGTP at the neurite tip (Winans et al., 2016). In addition to the above limitation, the frequency of actin waves has been shown to decrease after neurons have been cultured for 3–4 days *in vitro* (Flynn et al., 2009; Ruthel and Banker, 1999); nevertheless, RanGTP remains enriched at the neurite tip in neurons that have been cultured for more than 4 days (data not shown). One interesting candidate for this anchoring protein is RanGAP1, which has been observed to localize to the tips of growing axons of DRG neurons (Yudin et al., 2008). Given that importin-β has been shown to inhibit the RanGAP1-stimulated hydrolysis of RanGTP (Floer and Blobel, 1996) and the observation that the importin-β–Ran complex is present in neuronal cytoplasm (Chen et al., 2017), it is possible that the RanGAP1 anchors RanGTP at the neurite tip without catalyzing the hydrolysis of GTP. Using RanGAP1 as the anchoring protein would also provide a convenient inactivation mechanism once the need for a RanGTP enrichment at the neurite tip is no longer required.

MATERIALS AND METHODS

Antibodies and reagents

Anti-RanGTP antibody (AR-12) was a kind gift from Ian Macara (Department of Cell & Developmental Biology, Vanderbilt University, USA) (Richards et al., 1995). Mouse anti-β-III-tubulin antibody TUJ1 (801202) and mouse anti-neurofilament monoclonal antibody SMI312 (837904) were purchased from Biolegend (San Diego, CA). Mouse anti-α-tubulin antibody (DM1A) was from Millipore (Billerica, MA). Alexa Fluor-conjugated phalloidin, Alexa Fluor-conjugated secondary antibodiesc, cytochalasin D (PHZ1063) and MitoTracker Red were from Thermo Fisher Scientific (Waltham, MA).

Expression plasmid construction

The Ran-expressing plasmids (pCAG-AcGFP-RanWT and pCAG-AcGFP-RanT24N) were cloned by inserting wild-type Ran or RanT24N obtained from pWT-Ran-V5-His-TOPO or pT24N-Ran-V5-His-TOPO using KpnI and PmeI into KpnI- and SmaI-digested pCAG-AcGFP1-C3 vector. pWT-Ran-V5-His-TOPO and pT24N-Ran-V5-His-TOPO were kindly provided by Richard Cerione (Department of Chemistry & Chemical Biology,

Journal of Cell Science (2020) 133, jcs241992. doi:10.1242/jcs.241992

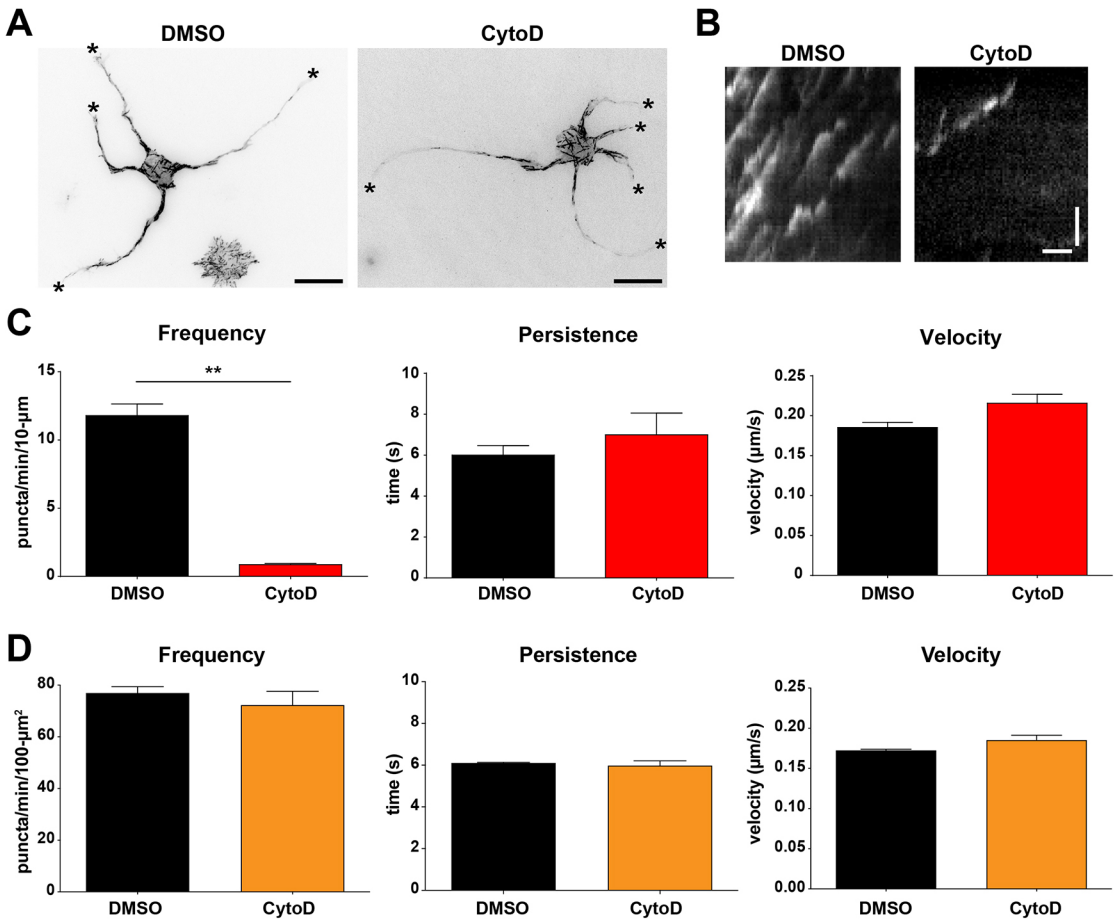

Fig. 6. Disrupting actin waves reduces the formation of non-centrosomal microtubule plus-ends at the neurite tip. (A) Representative maximum projection images (over a 2 min period) of 1DIV EB3–mCherry-expressing hippocampal neurons treated with DMSO (left) or 2.5 µM cytochalasin D (right) for 6 h. Hippocampal neurons were transfected with plasmids expressing EB3–mCherry and EGFP immediately before plating, incubated for 18 h, and treated with DMSO or 2.5 µM cytochalasin D for 6 h before being subjected to live-cell imaging. Asterisks mark the tips of the neurites. Scale bars: 20 µm. (B) Representative kymographs of EB3–mCherry at the neurite tip in DMSO- (left) or 2.5 µM cytochalasin D-treated (right) neurons. The vertical scale bar in the kymograph represents 2 µm and horizontal scale bar represents 10 s. (C,D) Quantification of EB3–mCherry dynamics at the neurite tip (C) or in the soma (D) in DMSO- or 2.5 µM cytochalasin D-treated neurons. $^{**}P<0.01$ (two-tailed Student's *t*-test). Error bars represent s.e.m. from 3 independent experiments, with more than 45 neurites or somata analyzed for each condition.

Cornell University, USA) (Ly et al., 2010). pCAG-AcGFP-RanQ69L was cloned by inserting RanQ69L obtained from pmCherry-C1-RanQ69L using BamHI and HindIII into pCAG-AcGFP1-C1 digested with the same enzymes. pCAG-IRES-EGFP, which expresses the cytosolic EGFP, was cloned by replacing the CMV promoter of pcDNA3.1(+)-IRES-EGFP (Addgene #51406) with the CAG promoter using SnaBI and NheI. pmCherry-C1-RanQ69L was Addgene plasmid #30309, deposited by Jay Brenman (Kazgan et al., 2010). pCAG-EB3-mCherry was cloned by replacing the CMV promoter of mCherry-EB3-7 (Addgene #55037) with the CAG promoter using SnaBI and HindIII.

pTriEx-NTOM20-mVenus-LOV2wt and pTriEx-mCherry-ZDK1 and pTriEx-PA-Rac1-I539E were kindly provided by Klaus Hahn (Wang et al., 2016). pTriEx-NTOM20-mVenus-LOV2-I539E was constructed by PCR amplifying LOV2-I539E from pTriEx-PA-Rac1-I539E, digested with BamHI/EcoRV, and ligated into BamHI/HindIII digested pTriEx-NTOM20-mVenus-LOV2wt vector. The HindIII cut site of BamHI/HindIII-digested pTriEx-NTOM20-mVenus-LOV2wt vector was blunted by Klenow fragment enzyme before ligation. The pTriEx-mCherry-ZDK1-RanQ69L and pTriEx-mCherry-ZDK1-RanT24N plasmids were cloned by inserting PCR amplified RanQ69L from pmCherry-C1-RanQ69L and PCR amplified RanT24N from pCAG-AcGFP-RanT24N into HindIII/XhoI digested pTriEx-mCherry-ZDK1 plasmid. A stop codon between ZDK1 and RanQ69L (or RanT24N) was removed by NotI/HindIII digestion, followed by ends blunting using Klenow fragment and self-ligation.

Neuron culture and transfection

All animal experimental procedures were approved by the Institutional Animal Care and Use Committee (IACUC) and in accordance with the Guide for the Care and Use of Laboratory Animals of National Chiao Tung University. Dissociated hippocampal and cortical neuron cultures were prepared as previously described with slight modification (Chen et al., 2017). Briefly, hippocampi or cortexes from E17.5 mouse embryos were dissected, digested with trypsin-EDTA and triturated. Dissociated neurons were seeded onto poly-L-lysine-coated coverslips (2.5×10^3 cells/cm^2 for low-density cultures and 3×10^4 cells/cm^2 for regular culture). Plasmids were introduced into neurons using Nucleofector II (Lonza, Basel, Switzerland) immediately before seeding or using Lipofectamine 2000 (Thermo Fisher Scientific) at the indicated number of days *in vitro*. Lipofectamine transfected cells were incubated for 4 h and the medium containing the transfection mixture was then replaced with cortical neuron-conditioned neurobasal medium (Thermo Fisher Scientific, 21103049) (low-density cultures) or fresh neurobasal medium plus B27 supplement (regular culture).

HeLa cell synchronization and transfection

HeLa cells were purchased from The Bioresource Collection and Research Center (BCRC) in Taiwan and routinely checked for mycoplasma contamination using the DAPI nuclear stain and fluorescence microscopy. A total of 7×10^4 HeLa cells were seeded per well in a 24-well plate. At 6–8 h after seeding, the growth medium (MEM, Thermo Fisher Scientific, 61100) was replaced with

2 mM thymidine-containing growth medium and incubated for 16 h. After this first thymidine block, cells were released and allowed to progress through cell cycle for 4 h. At this point, Lipofectamine 2000-based transfection was performed. At 4 h post transfection, the growth medium was again replaced with 2 mM thymidine-containing growth medium and incubated for another 16 h. After the second thymidine block, HeLa cells were released and incubated for 10 h before being fixed for subsequent analyses.

Indirect immunofluorescence staining

Cells were fixed with 3.7% formaldehyde for 15 min at 37°C and then washed three times with PBS. The fixed cells were permeabilized with 0.25% Triton X-100 in PBS for 5 min at room temperature and washed with PBS three times. Cells were then blocked with 10% BSA in PBS for 30 min at 37°C. Coverslips with cells were then incubated for 1 h at 37°C with primary antibodies: anti-α-tubulin (1:1000), anti-β-III-tubulin (1:4000), anti-RanGTP (1:100), and anti-neurofilament (1:1000). After primary antibody incubation, cells were incubated with Alexa Fluor-conjugated secondary antibodies (1:1000). All antibodies were diluted in 2% BSA in PBS. Coverslips with cells attached were washed with PBS three times and mounted using Fluoromount onto glass slides.

Image acquisition

Images of HeLa cells stained for immunofluorescence microscopy were acquired on an Olympus IX-71 inverted microscope equipped with a 40×0.95 NA Plan Apochromat objective lens, a CoolLED epi-fluorescence light source, a Hamamatsu ORCA-R2 camera, and MetaMorph software 7.6.5.0. Immunofluorescence stained neurons were acquired on a Nikon Eclipse-Ti inverted microscope equipped with a 60×1.49 NA Plan Apochromat objective lens, an Intensilight epi-fluorescence light source, a Photometrics CoolSNAP HQ2 camera, and Nikon NIS-Elements software 4.13.05.

Live-cell imaging was performed on a Nikon Eclipse-Ti inverted microscope equipped with a 60×1.49 NA Plan Apochromat objective lens, a Photometrics CoolSNAP HQ2 camera, a built-in Perfect Focus system, a Tokai Hit TIZHB live cell chamber, and Nikon NIS-Elements software 4.13.05. For quantifying MT dynamics, EB3–mCherry was excited using a TIRF illuminator and a 561nm DPSS laser; images were acquired every 500 ms over a 1- or 2-min period. For examining actin waves and the migration of Ran mutants along the neurite, AcGFP–Ran molecules were excited using an Intensilight epi-fluorescence light source; both DIC and fluorescence images were acquired every 3 min over a 4-h period.

Photoactivation of RanTRAP

The photoactivation experiments were performed on the same microscope as the live-cell imaging experiments. A 60×1.49 NA Plan Apochromat objective lens and an Intensilight epi-fluorescence illuminator were used for photoactivation. The field diaphragm was closed down to the minimal size (~40 µm in diameter) during the photoactivation period. A Nikon stock FITC filter set and the 1/32 ND filter were used to condition the photoactivation light. A 24-pulse regime (24 pulses of 80 ms irradiation time with 5 s interval between pulses) was carried out using NIS-Element software 4.13.05. All the photoactivation regions selected were more than 15 µm away from the soma or more than 15 µm away from the tip of the neurite.

Image analysis

For analyzing the distribution of RanGTP signals along the neurite (linescan analyses), only neuronal protrusions that were β-III-tubulin positive, and were longer than the diameter of its soma were considered as neurites. In addition, only neurites not intersecting other neurites were included in the analysis. The analysis was performed by manually tracing neurites from the soma edge to the neurite tip (neurites without a growth cone) or to the 'wrist' of the growth cone (neurites with a growth cone) with a segment line 0.55 µm in width in the RanGTP or EGFP channel using ImageJ v1.49. The RanGTP signal was then normalized against the cytosolic EGFP signal. To identify the center of the actin wave for setting the origin for Fig. S6B, 3–5-µm-wide linescans along the neurite shaft with the highest intensity in the Alexa Fluor 405-conjugated phalloidin channel were used.

For EB3–mCherry comets analysis in the neurite, NIS-Elements software 4.13.05 was used to generate the kymograph for the EB3–mCherry channel. A window 40 µm (for photoactivation experiments) or 10 µm (for all other experiments) in length and 0.77 µm in width was used to generate the kymograph. Only EB3–mCherry movements that could be followed clearly for equal or more than 4 frames (1.5 s) were defined as an event. The emanating frequency of EB3–mCherry was quantified from the kymograph by manually counting the number of EB3–mCherry events per minute. The velocity and persistence time of EB3–mCherry were quantified from the kymograph by drawing a line along an EB3–mCherry event. For analysis of EB3–mCherry comets in the soma, the ImageJ plugin TrackMate v5.1.0 was used (Tinevez et al., 2017). The soma region was manually selected, and the 'Differences of Gaussian (DoG)' detector model as well as the 'Linear motion LAP tracker' method were used to quantify EB3 dynamics. Only EB3–mCherry movements that could be tracked for equal or more than 4 frames (1.5 s) were included in the analysis.

For Ran mutant and actin wave co-migration analysis, only neurites with actin waves were included in the analysis. The position of the actin wave along the neurite shaft was manually determined from the DIC images. The analysis was performed by first manually tracing neurites from the edge of the soma to the neurite tip (for neurites without a growth cone) or to the wrist of the growth cone (for neurites with a growth cone) with a segment line 0.55 µm in width. This manually traced line was then used to perform linescan analysis in the AcGFP-Ran channel or the DIC channel by ImageJ v1.49. The signal intensity of AcGFP–Ran was normalized so that the highest intensity along the manually traced segment was set to 1 and lowest intensity to 0.

For quantifying AcGFP–Ran intensity change over time, a circular ROI (4 pixels in diameter) was created at the center of an actin wave-containing neurite using ImageJ v1.49. The intensity of AcGFP in this ROI was measured every 3 min from 15 min before the arrival of the actin waves (−15 min) to 15 min after the actin wave has passed (15 min). The intensity of AcGFP was then normalized against the value at the −15 min time point.

Statistical analysis

All statistical analyses were performed using GraphPad Prism 7 with the indicated statistical methods.

Acknowledgements

We thank Prof. Klaus Hahn for providing the pTriEx-NTOM20-mVenus-LOV2wt and pTriEx-mCherry-ZDK1 plasmids. We are grateful to Prof. Richard Cerione for providing the pWT-Ran-V5-His-TOPO and pT24N-Ran-V5-His-TOPO plasmids. We also would like to thank Prof. Ian Macara for providing the anti-RanGTP antibody.

Competing interests

The authors declare no competing or financial interests.

Author contributions

Conceptualization: E.H.; Methodology: Y.-A.H., C.-H.H.; Formal analysis: Y.-A.H., C.-H.H., H.-C.C., P.-Y.H., C.T.H., W.-L.L., E.H.; Investigation: Y.-A.H., C.-H.H., H.-C.C., P.-Y.H., C.T.H., W.-L.L.; Writing - original draft: Y.-A.H., C.-H.H., E.H.; Writing - review & editing: E.H.; Visualization: Y.-A. H., C.-H.H., H.-C.C., P.-Y.H., C.T.H., W.-L.L., E.H.; Supervision: E.H.; Funding acquisition: E.H.

Funding

This work was supported by grants from Ministry of Science and Technology, Taiwan (MOST 105-2320-B-009-005-MY3 and MOST 108-2628-B-009-003) and the 'Center for Intelligent Drug Systems and Smart Bio-devices (IDS^{2}B)' from The Featured Areas Research Center Program within the framework of the Higher Education Sprout Project by the Ministry of Education (MOE) in Taiwan.

Supplementary information

Supplementary information available online at
http://jcs.biologists.org/lookup/doi/10.1242/jcs.241992.supplemental

Peer review history

The peer review history is available online at
https://jcs.biologists.org/lookup/doi/10.1242/jcs.241992.reviewer-comments.pdf.

References

Bartolini, F. and Gundersen, G. G. (2006). Generation of noncentrosomal microtubule arrays. *J. Cell Sci.* **119**, 4155-4163. doi:10.1242/jcs.03227

Brouhard, G. J. and Rice, L. M. (2018). Microtubule dynamics: an interplay of biochemistry and mechanics. *Nat. Rev. Mol. Cell Biol.* **19**, 451-463. doi:10.1038/s41580-018-0009-y

Chen, W.-S., Chen, Y.-J., Huang, Y.-A., Hsieh, B.-Y., Chiu, H.-C., Kao, P.-Y., Chao, C.-Y. and Hwang, E. (2017). Ran-dependent TPX2 activation promotes acentrosomal microtubule nucleation in neurons. *Sci. Rep.* **7**, 42297. doi:10.1038/srep42297

Cheng, L., Lemmon, S. and Lemmon, V. (2005). RanBPM is an L1-interacting protein that regulates L1-mediated mitogen-activated protein kinase activation. *J. Neurochem.* **94**, 1102-1110. doi:10.1111/j.1471-4159.2005.03254.x

Chia, J. X., Efimova, N. and Svitkina, T. M. (2016). Neurite outgrowth is driven by actin polymerization even in the presence of actin polymerization inhibitors. *Mol. Biol. Cell* **27**, 3687-3790. doi:10.1091/mbc.e16-04-0253

Clarke, P. R. and Zhang, C. (2008). Spatial and temporal coordination of mitosis by Ran GTPase. *Nat. Rev. Mol. Cell Biol.* **9**, 464-477. doi:10.1038/nrm2410

Cunha-Ferreira, I., Chazeau, A., Buijs, R. R., Stucchi, R., Will, L., Pan, X., Adolfs, Y., van der Meer, C., Wolthuis, J. C., Kahn, O. I. et al. (2018). The HAUS complex is a key regulator of non-centrosomal microtubule organization during neuronal development. *Cell Rep.* **24**, 791-800. doi:10.1016/j.celrep.2018.06.093

Deng, M., Suraneni, P., Schultz, R. M. and Li, R. (2007). The Ran GTPase mediates chromatin signaling to control cortical polarity during polar body extrusion in mouse oocytes. *Dev. Cell* **12**, 301-308. doi:10.1016/j.devcel.2006.11.008

Desai, A. and Mitchison, T. J. (1997). Microtubule polymerization dynamics. *Annu. Rev. Cell Dev. Biol.* **13**, 83-117. doi:10.1146/annurev.cellbio.13.1.83

Dickson, T. C., Mintz, C. D., Benson, D. L. and Salton, S. R. J. (2002). Functional binding interaction identified between the axonal CAM L1 and members of the ERM family. *J. Cell Biol.* **157**, 1105-1112. doi:10.1083/jcb.200111076

Floer, M. and Blobel, G. (1996). The nuclear transport factor karyopherin beta binds stoichiometrically to Ran-GTP and inhibits the Ran GTPase activating protein. *J. Biol. Chem.* **271**, 5313-5316. doi:10.1074/jbc.271.10.5313

Flynn, K. C., Pak, C. W., Shaw, A. E., Bradke, F. and Bamburg, J. R. (2009). Growth cone-like waves transport actin and promote axonogenesis and neurite branching. *Dev. Neurobiol.* **69**, 761-779. doi:10.1002/dneu.20734

Gorlich, D. and Mattaj, I. W. (1996). Nucleocytoplasmic transport. *Science* **271**, 1513-1519. doi:10.1126/science.271.5255.1513

Gruss, O. J., Carazo-Salas, R. E., Schatz, C. A., Guarguaglini, G., Kast, J., Wilm, M., Le Bot, N., Vernos, I., Karsenti, E. and Mattaj, I. W. (2001). Ran induces spindle assembly by reversing the inhibitory effect of importin alpha on TPX2 activity. *Cell* **104**, 83-93. doi:10.1016/S0092-8674(01)00193-3

Hanz, S., Perlson, E., Willis, D., Zheng, J.-Q., Massarwa, R., Huerta, J. J., Koltzenburg, M., Kohler, M., van-Minnen, J., Twiss, J. L. et al. (2003). Axoplasmic importins enable retrograde injury signaling in lesioned nerve. *Neuron* **40**, 1095-1104. doi:10.1016/S0896-6273(03)00770-0

Harper, S. M., Christie, J. M. and Gardner, K. H. (2004). Disruption of the LOV-Jalpha helix interaction activates phototropin kinase activity. *Biochemistry* **43**, 16184-16192. doi:10.1021/bi048092i

Huala, E., Oeller, P. W., Liscum, E., Han, I. S., Larsen, E. and Briggs, W. R. (1997). Arabidopsis NPH1: a protein kinase with a putative redox-sensing domain. *Science* **278**, 2120-2123. doi:10.1126/science.278.5346.2120

Inagaki, N. and Katsuno, H. (2017). Actin waves: origin of cell polarization and migration? *Trends Cell Biol.* **27**, 515-526. doi:10.1016/j.tcb.2017.02.003

Kahana, J. A. and Cleveland, D. W. (1999). Beyond nuclear transport. Ran-GTP as a determinant of spindle assembly. *J. Cell Biol.* **146**, 1205-1210. doi:10.1083/jcb.146.6.1205

Kakumoto, T. and Nakata, T. (2013). Optogenetic control of PIP3: PIP3 is sufficient to induce the actin-based active part of growth cones and is regulated via endocytosis. *PLoS ONE* **8**, e70861. doi:10.1371/journal.pone.0070861

Katsuno, H., Toriyama, M., Hosokawa, Y., Mizuno, K., Ikeda, K., Sakumura, Y. and Inagaki, N. (2015). Actin migration driven by directional assembly and disassembly of membrane-anchored actin filaments. *Cell Rep.* **12**, 648-660. doi:10.1016/j.celrep.2015.06.048

Kazgan, N., Williams, T., Forsberg, L. J. and Brenman, J. E. (2010). Identification of a nuclear export signal in the catalytic subunit of AMP-activated protein kinase. *Mol. Biol. Cell* **21**, 3433-3442. doi:10.1091/mbc.e10-04-0347

Keating, T. J. and Borisy, G. G. (1999). Centrosomal and non-centrosomal microtubules. *Biol. Cell* **91**, 321-329. doi:10.1111/j.1768-322X.1999.tb01090.x

Klebe, C., Bischoff, F. R., Ponstingl, H. and Wittinghofer, A. (1995). Interaction of the nuclear GTP-binding protein Ran with its regulatory proteins RCC1 and RanGAP1. *Biochemistry* **34**, 639-647. doi:10.1021/bi00002a031

Lakshmana, M. K., Hayes, C. D., Bennett, S. P., Bianchi, E., Reddy, K. M., Koo, E. H. and Kang, D. E. (2012). Role of RanBP9 on amyloidogenic processing of APP and synaptic protein levels in the mouse brain. *FASEB J.* **26**, 2072-2083. doi:10.1096/fj.11-196709

Leask, A., Obrietan, K. and Stearns, T. (1997). Synaptically coupled central nervous system neurons lack centrosomal gamma-tubulin. *Neurosci. Lett.* **229**, 17-20. doi:10.1016/S0304-3940(97)00412-6

Ly, T. K., Wang, J., Pereira, R., Rojas, K. S., Peng, X., Feng, Q., Cerione, R. A. and Wilson, K. F. (2010). Activation of the Ran GTPase is subject to growth factor regulation and can give rise to cellular transformation. *J. Biol. Chem.* **285**, 5815-5826. doi:10.1074/jbc.M109.071886

Mencarelli, C., Nitarska, J., Kroecher, T., Ferraro, F., Massey, K., Riccio, A. and Pichaud, F. (2018). RanBP1 couples nuclear export and Golgi regulation through LKB1 to promote cortical neuron polarity. *Cell Rep.* **24**, 2529-2539.e4. doi:10.1016/j.celrep.2018.07.107

Moore, W. J., Zhang, C. and Clarke, P. R. (2002). Targeting of RCC1 to chromosomes is required for proper mitotic spindle assembly in human cells. *Curr. Biol.* **12**, 1442-1447. doi:10.1016/S0960-9822(02)01076-X

Muroyama, A. and Lechler, T. (2017). Microtubule organization, dynamics and functions in differentiated cells. *Development* **144**, 3012-3021. doi:10.1242/dev.153171

Nakagawa, H., Koyama, K., Murata, Y., Morito, M., Akiyama, T. and Nakamura, Y. (2000). EB3, a novel member of the EB1 family preferentially expressed in the central nervous system, binds to a CNS-specific APC homologue. *Oncogene* **19**, 210-216. doi:10.1038/sj.onc.1203308

Nakamura, M., Masuda, H., Horii, J., Kuma, K.-I., Yokoyama, N., Ohba, T., Nishitani, H., Miyata, T., Tanaka, M. and Nishimoto, T. (1998). When overexpressed, a novel centrosomal protein, RanBPM, causes ectopic microtubule nucleation similar to gamma-tubulin. *J. Cell Biol.* **143**, 1041-1052. doi:10.1083/jcb.143.4.1041

Nguyen, M. M., McCracken, C. J., Milner, E. S., Goetschius, D. J., Weiner, A. T., Long, M. K., Michael, N. L., Munro, S. and Rolls, M. M. (2014). Gamma-tubulin controls neuronal microtubule polarity independently of Golgi outposts. *Mol. Biol. Cell* **25**, 2039-2050. doi:10.1091/mbc.e13-09-0515

Ori-McKenney, K. M., Jan, L. Y. and Jan, Y.-N. (2012). Golgi outposts shape dendrite morphology by functioning as sites of acentrosomal microtubule nucleation in neurons. *Neuron* **76**, 921-930. doi:10.1016/j.neuron.2012.10.008

Petry, S., Groen, A. C., Ishihara, K., Mitchison, T. J. and Vale, R. D. (2013). Branching microtubule nucleation in Xenopus egg extracts mediated by augmin and TPX2. *Cell* **152**, 768-777. doi:10.1016/j.cell.2012.12.044

Richards, S. A., Lounsbury, K. M. and Macara, I. G. (1995). The C terminus of the nuclear RAN/TC4 GTPase stabilizes the GDP-bound state and mediates interactions with RCC1, RAN-GAP, and HTF9A/RANBP1. *J. Biol. Chem.* **270**, 14405-14411. doi:10.1074/jbc.270.24.14405

Ruthel, G. and Banker, G. (1998). Actin-dependent anterograde movement of growth-cone-like structures along growing hippocampal axons: a novel form of axonal transport? *Cell Motil. Cytoskeleton* **40**, 160-173. doi:10.1002/(SICI)1097-0169(1998)40:2<160::AID-CM5>3.0.CO;2-J

Ruthel, G. and Banker, G. (1999). Role of moving growth cone-like "wave" structures in the outgrowth of cultured hippocampal axons and dendrites. *J. Neurobiol.* **39**, 97-106. doi:10.1002/(SICI)1097-4695(199904)39:1<97::AID-NEU8>3.0.CO;2-Z

Salomon, M., Christie, J. M., Knieb, E., Lempert, U. and Briggs, W. R. (2000). Photochemical and mutational analysis of the FMN-binding domains of the plant blue light receptor, phototropin. *Biochemistry* **39**, 9401-9410. doi:10.1021/bi000585+

Sanchez, A. D. and Feldman, J. L. (2017). Microtubule-organizing centers: from the centrosome to non-centrosomal sites. *Curr. Opin. Cell Biol.* **44**, 93-101. doi:10.1016/j.ceb.2016.09.003

Sanchez-Huertas, C., Freixo, F., Viais, R., Lacasa, C., Soriano, E. and Luders, J. (2016). Non-centrosomal nucleation mediated by augmin organizes microtubules in post-mitotic neurons and controls axonal microtubule polarity. *Nat. Commun.* **7**, 12187. doi:10.1038/ncomms12187

Sepp, K. J., Hong, P., Lizarraga, S. B., Liu, J. S., Mejia, L. A., Walsh, C. A. and Perrimon, N. (2008). Identification of neural outgrowth genes using genome-wide RNAi. *PLoS Genet.* **4**, e1000111. doi:10.1371/journal.pgen.1000111

Stiess, M., Maghelli, N., Kapitein, L. C., Gomis-Ruth, S., Wilsch-Brauninger, M., Hoogenraad, C. C., Tolic-Norrelykke, I. M. and Bradke, F. (2010). Axon extension occurs independently of centrosomal microtubule nucleation. *Science* **327**, 704-707. doi:10.1126/science.1182179

Tinevez, J.-Y., Perry, N., Schindelin, J., Hoopes, G. M., Reynolds, G. D., Laplantine, E., Bednarek, S. Y., Shorte, S. L. and Eliceiri, K. W. (2017). TrackMate: an open and extensible platform for single-particle tracking. *Methods* **115**, 80-90. doi:10.1016/j.ymeth.2016.09.016

Wang, H. and Hahn, K. M. (2016). LOVTRAP: a versatile method to control protein function with light. *Curr. Protoc. Cell Biol.* **73**, 21.10.1-21.10.14. doi:10.1002/cpcb.12

Wang, H., Vilela, M., Winkler, A., Tarnawski, M., Schlichting, I., Yumerefendi, H., Kuhlman, B., Liu, R., Danuser, G. and Hahn, K. M. (2016). LOVTRAP: an optogenetic system for photoinduced protein dissociation. *Nat. Methods* **13**, 755-758. doi:10.1038/nmeth.3926

Winans, A. M., Collins, S. R. and Meyer, T. (2016). Waves of actin and microtubule polymerization drive microtubule-based transport and neurite growth before single axon formation. *eLife* **5**, e12387. doi:10.7554/eLife.12387

Woo, J. A., Roh, S. E., Lakshmana, M. K. and Kang, D. E. (2012). Pivotal role of RanBP9 in integrin-dependent focal adhesion signaling and assembly. *FASEB J.* **26**, 1672-1681. doi:10.1096/fj.11-194423

Yi, K., Unruh, J. R., Deng, M., Slaughter, B. D., Rubinstein, B. and Li, R. (2011). Dynamic maintenance of asymmetric meiotic spindle position through Arp2/3-

complex-driven cytoplasmic streaming in mouse oocytes. *Nat. Cell Biol.* **13**, 1252-1258. doi:10.1038/ncb2320

Yu, W., Centonze, V. E., Ahmad, F. J. and Baas, P. W. (1993). Microtubule nucleation and release from the neuronal centrosome. *J. Cell Biol.* **122**, 349-359. doi:10.1083/jcb.122.2.349

Yudin, D., Hanz, S., Yoo, S., Iavnilovitch, E., Willis, D., Gradus, T., Vuppalanchi, D., Segal-Ruder, Y., Ben-Yaakov, K., Hieda, M. Y. et al. (2008). Localized regulation of axonal RanGTPase controls retrograde injury signaling in peripheral nerve. *Neuron* **59**, 241-252. doi:10.1016/j.neuron.2008.05.029

Supplementary Figures

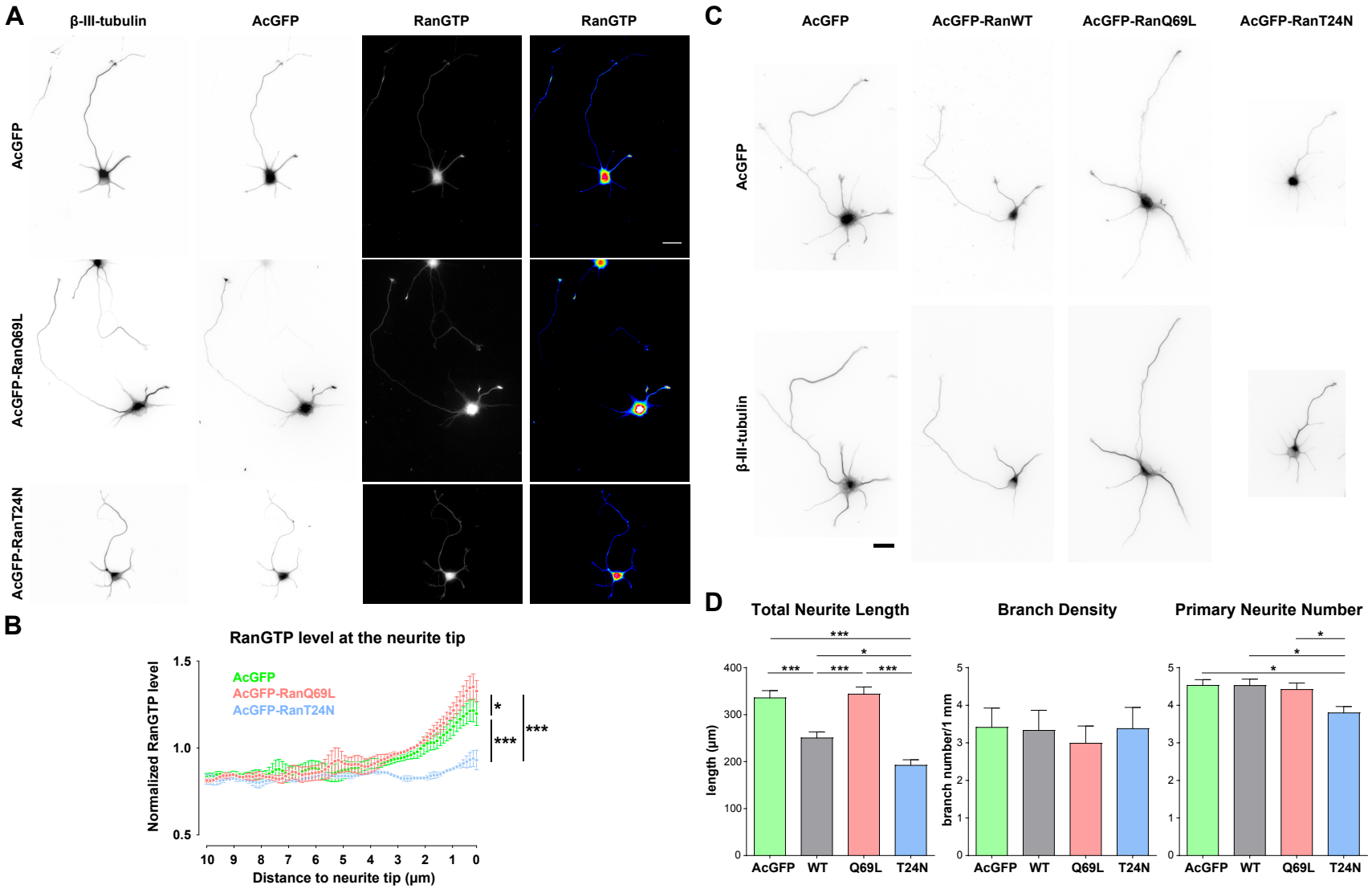

Figure S1. Ran mutants influence the level of RanGTP at the neurite tip and neuronal morphogenesis.
(A) Representative images of 2DIV low-density dissociated hippocampal neurons expressing AcGFP, AcGFP-RanQ69L, or AcGFP-RanT24N. β-III-tubulin, AcGFP, RanGTP, and pseudo-colored RanGTP channels are shown. All images have the same scale and the scale bar represents 20 μm. (B) Normalized RanGTP level linescans at the neurite tip (AcGFP is shown in green, AcGFP-RanQ69L in red, and AcGFP-RanT24N in blue). RanGTP intensity 0~10 μm from the neurite tip was normalized to the average RanGTP intensity along the entire neurite. The dots and error bars indicate mean and SEM from 3 independent experiments. At least 119 neurites from 3 independent experiments from each condition were analyzed. *** $p<0.001$, * $p<0.05$, two-way ANOVA followed by Tukey post-hoc test (RanGTP level 0~1 μm from the tip of the neurite). (C) Representative images of 2DIV low-density dissociated hippocampal neurons expressing AcGFP, AcGFP-RanWT, AcGFP-RanQ69L, or AcGFP-RanT24N. AcGFP (top) and β-III tubulin (bottom) channels are shown. All images have the same scale and the scale bar represents 20 μm. (D) Quantification of total neurite length (left), branch density (middle), and primary neurite number (right) in Ran expressing neurons. * $p<0.05$, *** $p<0.001$, one-way ANOVA followed by Tukey's post-hoc test. Error bars represent SEM from 3 independent experiments.

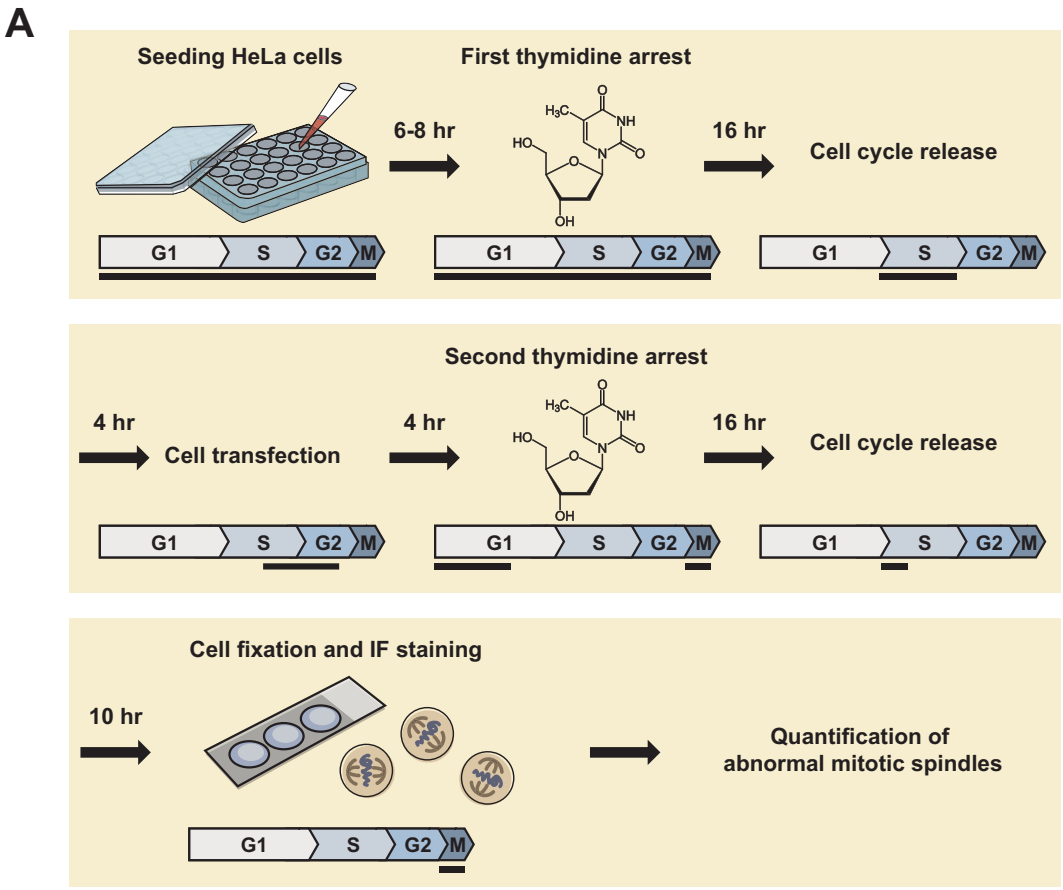

Figure S2. Functional validation of RanTRAP system in HeLa cells.
(A) Schematic procedure of double thymidine arrest to synchronize HeLa cells. The black horizontal bars indicate where in the cell cycle most cells are. (B) Representative images of synchronized mitotic HeLa cells with normal or abnormal spindles. Cells were stained with α-tubulin antibody (DM1A) and DAPI. The spindle morphology was categorized using the following criteria. A mitotic spindle containing two spindle poles and aligned chromosomes was categorized as "metaphase" spindle. A mitotic spindle containing two spindle poles and segregated chromosomes was categorized as "anaphase/telophase" spindle. A mitotic spindle containing two spindle poles and misaligned chromosomes was categorized as "bipolar spindle with misaligned chromosomes". A mitotic spindle containing more than two spindle poles was categorized as "multipolar spindle". A mitotic spindle containing only one spindle pole and radially arranged chromosomes was categorized as "monopolar spindle". The scale bar represents 10 μm. (C) Quantification of abnormal spindle occurrence. More than 50 mitotic HeLa cells were analyzed per condition per repeat. * $p<0.05$, ** $p<0.01$, *** $p<0.001$, one-way ANOVA followed by Tukey's multiple comparison test. Error bars represent SEM from 3 independent experiments.

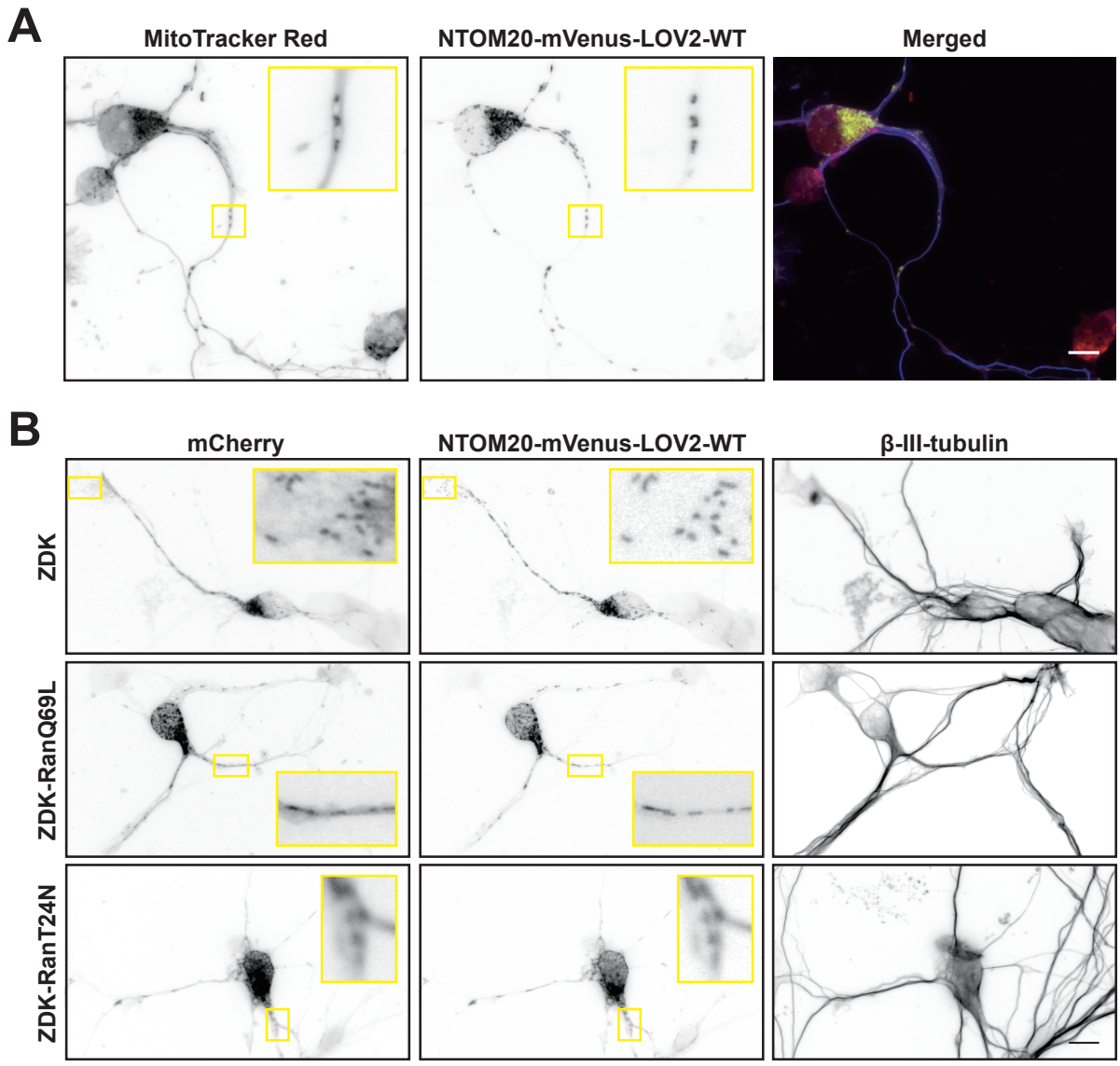

Figure S3. The RanTRAP system targets Ran to mitochondria along the neurite.
(A) Representative images of a mouse cortical neurons transfected with plasmid expressing NTOM20-mVenus-LOV2-WT (green in merged) at 2DIV, fixed and stained with MitoTracker Red (red in merged) and β-III-tubulin antibody (blue in merged) at 4DIV. (B) Representative images of mouse cortical neurons transfected with plasmids expressing NTOM20-mVenus-LOV2-WT and mCherry-ZDK (or mCherry-ZDK-RanQ69L or mCherry-RanT24N) at 2DIV, fixed and stained with the β-III-tubulin antibody at 4DIV. Insets show the magnified view of yellow boxed areas. All scale bars represent 10 μm.

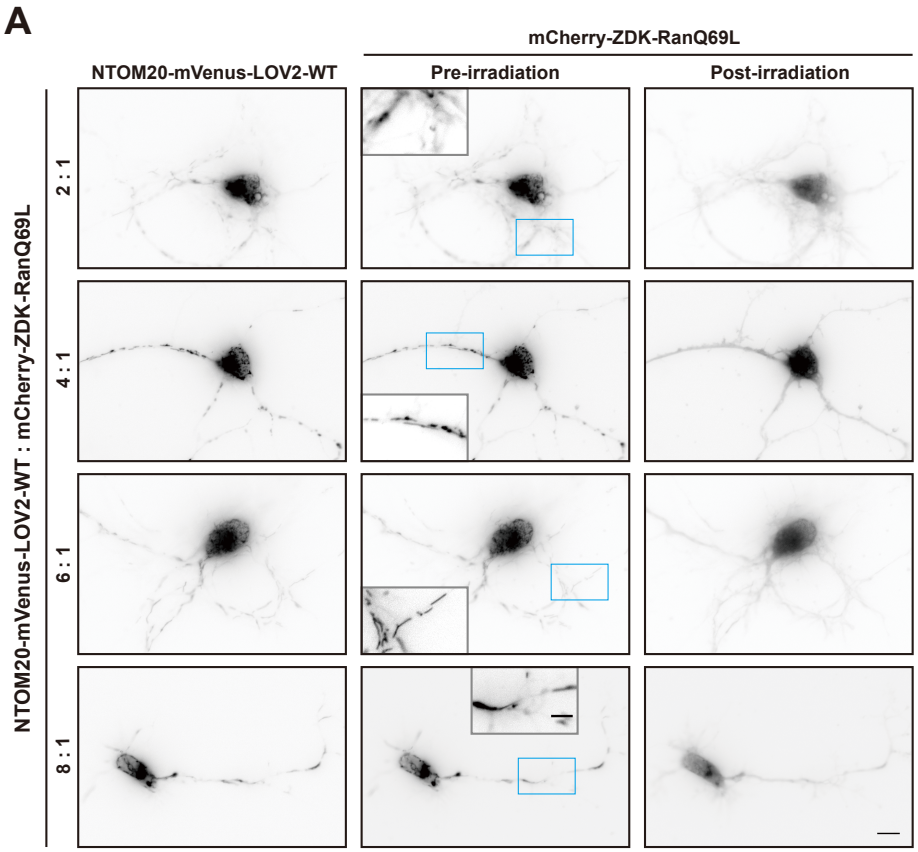

Figure S4. Optimizing the molar ratio of RanTRAP plasmids in neurons.
(A) Representative live cell images of 4DIV mouse cortical neurons co-expressing NTOM20-mVenus-LOV2-WT and mCherry-ZDK-RanQ69L. Neurons were transfected with various molar ratios of plasmid expressing NTOM20-mVenus-LOV2-WT and mCherry-ZDK -RanQ69L (LOV2:ZDK = 2:1, 4:1, 6:1, 8:1) at 2DIV, incubated for 2 days before subjected to live cell imaging. All images have the same scale and the scale bar represents 10 μm. The image insets show the magnified and contrast enhanced view of the area enclosed by the blue box, and the scale bar in the inset represents 5 μm. (B) Representative images showing the ROI (blue circle) where cytosolic mCherry-ZDK-RanQ69L level was quantified. Both live cell images show 4 DIV mouse cortical neurons expressing NTOM20-mVenus-LOV2-WT and mCherry-ZDK-RanQ69L for 2 days. Blue circular ROIs (1.1 μm in diameter) indicate where cytosolic mCherry-ZDK-RanQ69L signal was quantified from. The scale bar represents 4 μm. (C) Quantification of cytosolic mCherry-ZDK-RanQ69L level before and after photoactivation in selected ROI along the neurite in various molar ratio conditions. In the molar ratio 8:1 condition, most of the transfected neurons are unhealthy. As a result, this condition was excluded from the quantification. 13, 30, and 19 neurites were quantified in 2:1, 4:1, and 6:1 conditions, respectively. Box plot shows median, first and third quartile, and whiskers extend to the entire range of data. *** $p<0.001$, one-way ANOVA followed by Tukey's multiple comparison test. Since no statistically significant difference can be detected between the 4:1 and 6:1 condition, the molar ratio (4:1) that produced the higher signal of mCherry-ZDK-RanQ96L was chosen for subsequent experiments.

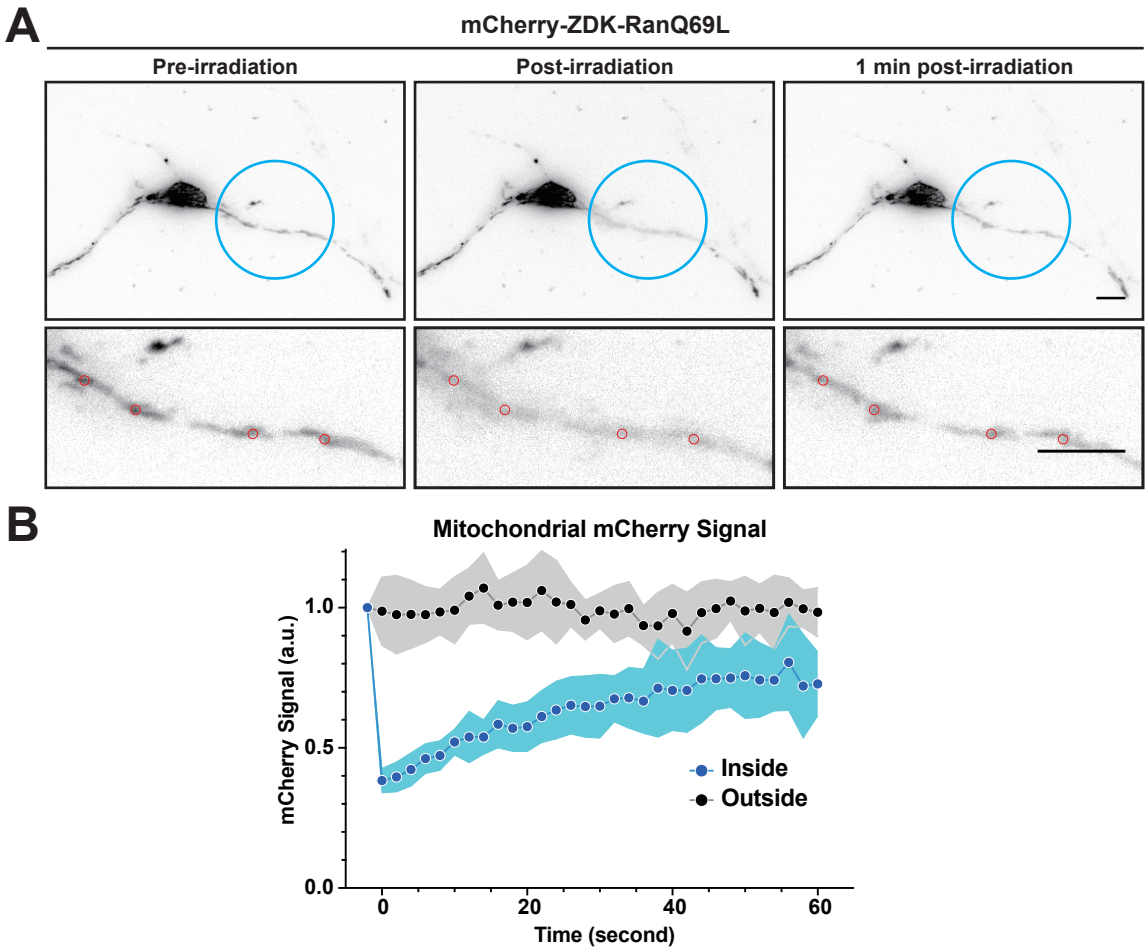

Figure S5. Local release of RanGTP-mimic mutant can be achieved in neurons.
(A) Mouse hippocampal neurons were co-transfected with plasmids expressing NTOM20-mVenus-LOV2-WT and mCherry-ZDK-RanQ69L at 3DIV, incubated for 1 days before subjected to live cell imaging. The blue circle indicated the region of photoactivation. Images on the bottom row show magnified images from the photoactivated region. The mCherry-ZDK-RanQ69L signal before (left), immediately after photoactivation (center), and 1 minute after photoactivation (right) are shown. All scale bars represent 10 μm. (B) Quantification of the mitochondria-localized mCherry-ZDK-RanQ69L signal over time from panel A. 4 selected ROIs (red circles in panel A) on the mitochondria inside (blue line) and outside (black line) the region of photoactivation are analyzed. Dots and shaded areas indicate mean and SD. Note that mCherry-ZDK-RanQ69L only dissociated from the mitochondria inside the photoactivated region.

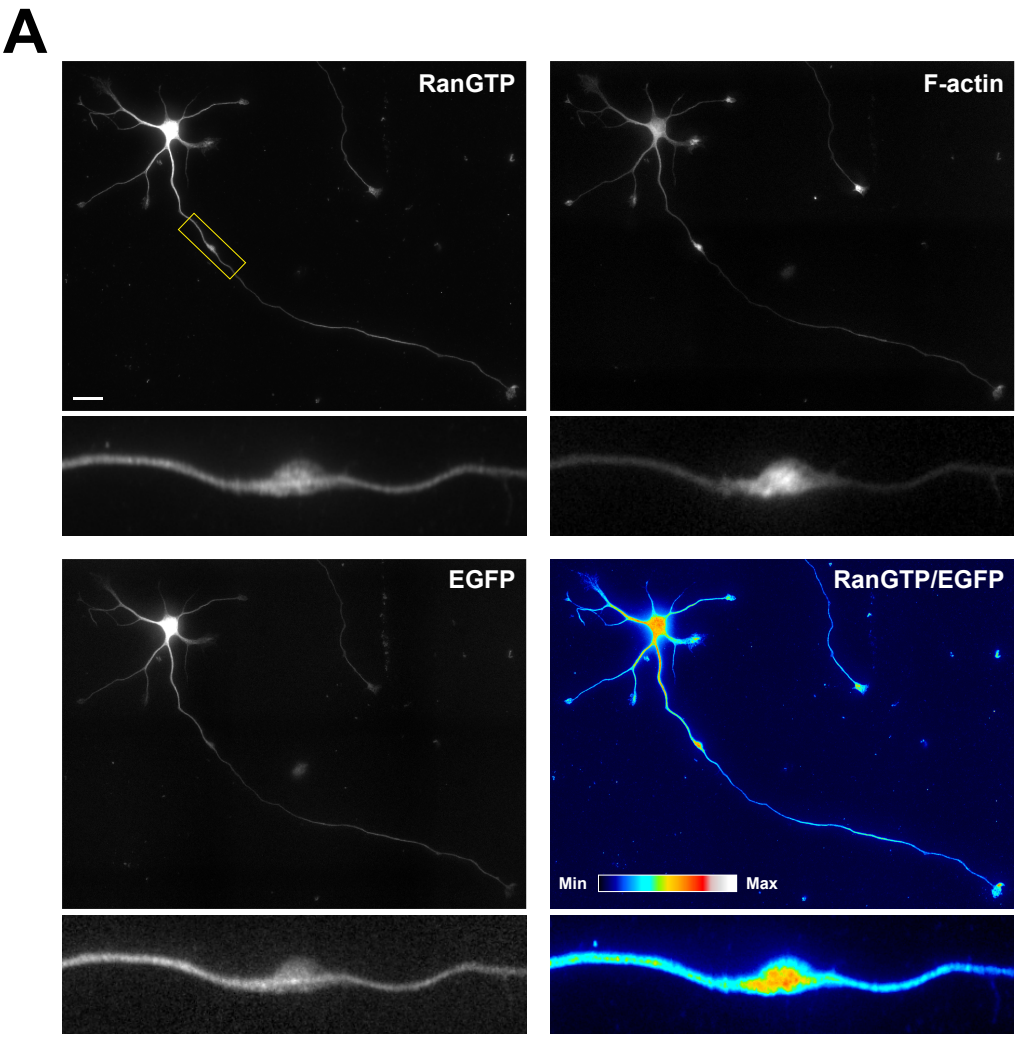

Figure S6. RanGTP level is elevated in the actin wave in neurons.

(A) Representative image of a 2DIV mouse hippocampal neurons expressing EGFP (bottom left) and immunofluorescence stained with antibody against RanGTP (top left) and phalloidin (top right). The ratio image of RanGTP/EGFP was pseudo-colored (bottom right). The boxed area was used to generated the magnified images. All images have the same scale and the scale bar represents 20 µm. (B) Cytoplasmic volume-normalized RanGTP intensity linescan along a 40 µm stretch centered at the actin wave (red) or a random location without the actin wave (blue) in 2DIV hippocampal neurons. The origin of the X-axis is selected using the neurite location with the highest phalloidin staining, negative or positive value of the X-axis indicate the neurite region towards or away from the soma. Dots and shaded areas indicate mean and SEM collected from 47 neurites, *** $p<0.001$, two-way ANOVA followed by Sidak post-hoc analysis between the red and the blue curves.

Movies

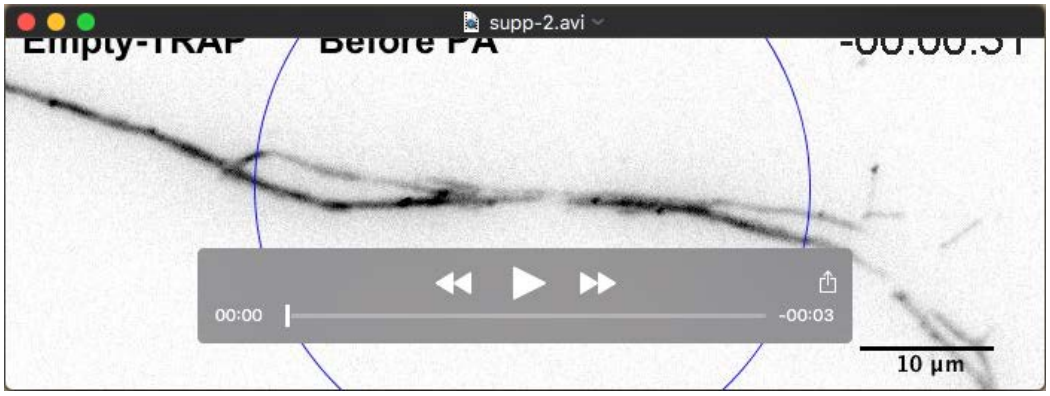

Movie 1. Non-centrosomal microtubule nucleation within the photoactivation region before and after photoactivation in a neuron expressing Empty-TRAP reagent.
Time-lapse video of a 4DIV hippocampal neuron expressing EB3-mCherry and Empty-TRAP before and after photoactivation. Only the EB3-mCherry channel is shown and the photoactivation region is indicated by the blue circle. The time stamp is expressed as hour:minute:second.
https://figshare.com/s/666c60c72185096510de

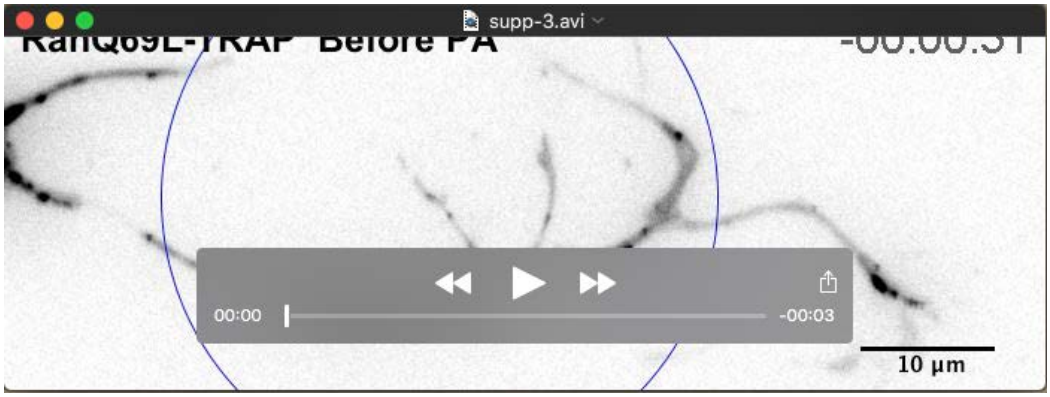

Movie 2. Non-centrosomal microtubule nucleation within the photoactivation region before and after photoactivation in a neuron expressing RanQ69L-TRAP reagent.
Time-lapse video of a 4DIV hippocampal neuron expressing EB3-mCherry and RanQ69L-TRAP before and after photoactivation. Only the EB3-mCherry channel is shown and the photoactivation region is indicated by the blue circle. The time stamp is expressed as hour:minute:second.
https://figshare.com/s/c5f185244b46f7f5084f

Journal of Cell Science • Supplementary information

Movie 3. Non-centrosomal microtubule nucleation within the photoactivation region before and after photoactivation in a neuron expressing RanT24N-TRAP reagent.
Time-lapse video of a 4DIV hippocampal neuron expressing EB3-mCherry and RanT24N-TRAP before and after photoactivation. Only the EB3-mCherry channel is shown and the photoactivation region is indicated by the blue circle. The time stamp is expressed as hour:minute:second.
https://figshare.com/s/14ac455f4bbf624e47a9

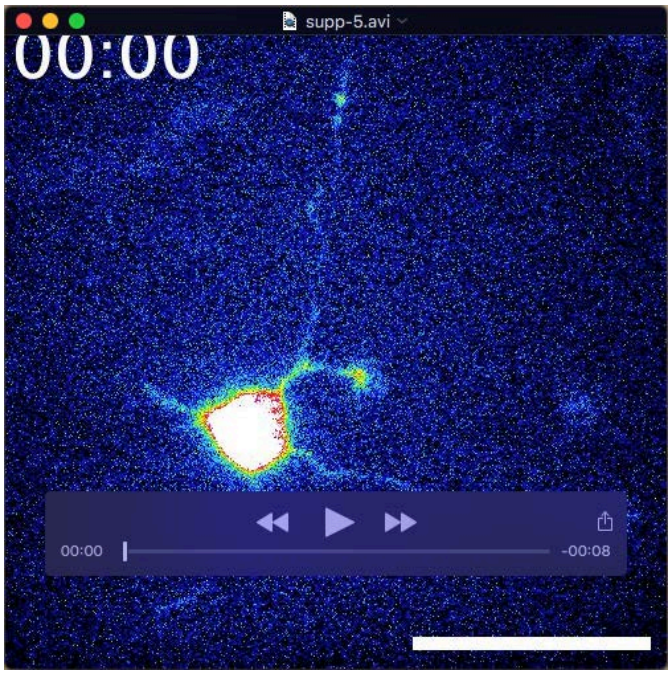

Movie 4. The motility of AcGFP-RanQ69L in a neuron actively generating actin waves.
Time-lapse video of a 2DIV cortical neuron expressing AcGFP-RanQ69L. The time stamp is expressed as hour:minute, and the scale bar represents 20 µm.
https://figshare.com/s/6f9f6194b710cfc04d7c

Journal of Cell Science • Supplementary information

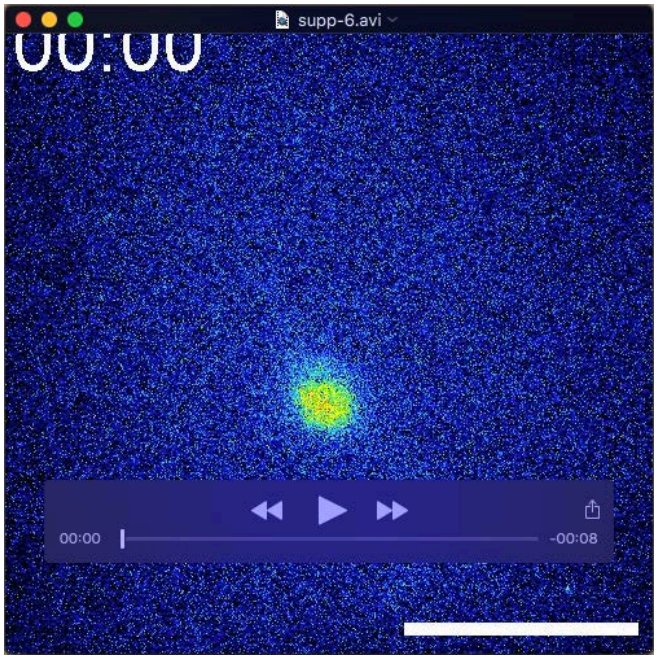

Movie 5. The motility of AcGFP-RanT24N in a neuron actively generating actin waves. Time-lapse video of a 2DIV cortical neuron expressing AcGFP-RanT24N. The time stamp is expressed as hour:minute, and the scale bar represents 20 µm.
https://figshare.com/s/82881e839edc8eba72f5

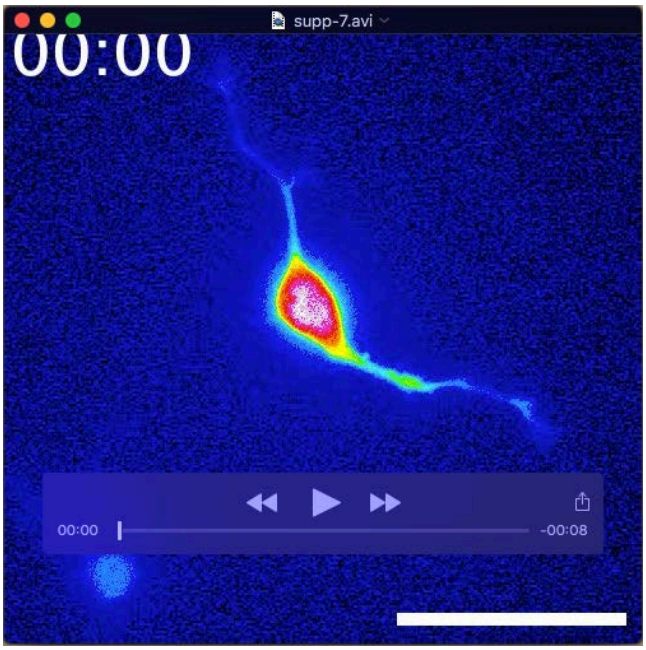

Movie 6. The motility of the cytosolic AcGFP in a neuron actively generating actin waves. Time-lapse video of a 2DIV cortical neuron expressing AcGFP. The time stamp is expressed as hour:minute, and the scale bar represents 20 µm.
https://figshare.com/s/eb87bee04f511a55cb7f

Journal of Cell Science • Supplementary information

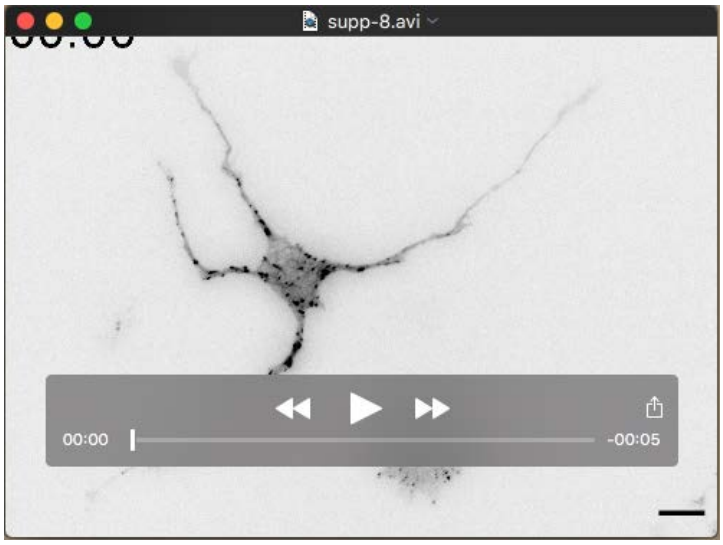

Movie 7. Microtubule dynamics in a neuron treated with DMSO.
Time-lapse video of a 1DIV EB3-mCherry-expressing hippocampal neuron after DMSO treatment for 6 hours. The time stamp is expressed as minute:second, and the scale bar represents 10 µm.
https://figshare.com/s/f7cab1b7df933e66a1ea

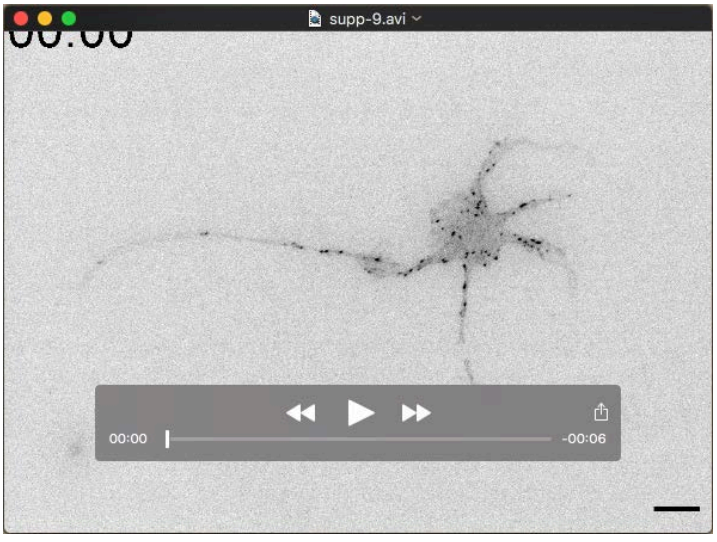

Movie 8. Microtubule dynamics in a neuron treated with cytochalasin D.
Time-lapse video of a 1DIV EB3-mCherry-expressing hippocampal neuron after cytochalasin D treatment for 6 hours. The time stamp is expressed as minute:second, and the scale bar represents 10 µm.
https://figshare.com/s/97d28fb22d71e2fc868b

Journal of Cell Science • Supplementary information